A posteriori error estimates and stopping criteria for space-time domain decomposition for two-phase flow between different rock types

Elyes Ahmed, Sarah Ali Hassan, Caroline Japhet, Michel Kern, Martin Vohralík

A posteriori error estimates and stopping criteria for space-time domain decomposition for two-phase flow between different rock types*

Elyes Ahmed[†‡] Sarah Ali Hassan[†] Caroline Japhet[‡] Michel Kern[†]
Martin Vohralík[†]

June 16, 2017

Abstract

We consider two-phase flow in a porous medium composed of two different rock types, so that the capillary pressure field is discontinuous at the interface between the rocks. This is a nonlinear and degenerate parabolic problem with nonlinear and discontinuous transmission conditions on the interface. We first describe a space-time domain decomposition method based on the optimized Schwarz waveform relaxation algorithm (OSWR) with Robin or Ventcell transmission conditions. Full numerical approximation is achieved by a finite volume scheme in space and the backward Euler scheme in time. We then derive a guaranteed and fully computable a posteriori error estimate which in particular takes into account the domain decomposition error. Precisely, at each iteration of the OSWR algorithm and on each linearization step, the estimate delivers a guaranteed upper bound on the error between the exact and the approximate solution. Furthermore, to make the OSWR algorithm efficient, the different error components given by the spatial discretization, the temporal discretization, the linearization, and the domain decomposition are distinguished. These ingredients are then used to design a stopping criterion for the OSWR algorithm as well as for the linearization iterations, which together lead to important computational savings. Numerical experiments illustrate the efficiency of our estimates and the performance of the OSWR algorithm with adaptive stopping criteria on a model problem in three space dimensions. Additionally, the results show how a posteriori error estimates can help determine the free Robin or Ventcell parameters.

Key words: two-phase Darcy flow, discontinuous capillary pressure, finite volume scheme, domain decomposition method, optimized Schwarz waveform relaxation, Robin and Ventcell transmission conditions, linearization, a posteriori error estimate, stopping criteria

1 Introduction

Two-phase flows in porous media are of interest in a number of situations, such as CO2 sequestration in saline aquifers, description of oil reservoirs, or gas migration around a nuclear waste repository in the subsurface, where natural and engineered barriers are used to isolate the radionuclides and to slow down their release from the storage site into the environment. In fact, one of the problems encountered when designing nuclear waste repositories is that of gas produced from the corrosion of metallic components and from the nuclear waste itself. The numerical simulation of such flows is a challenging task, in particular

*This work was supported by the French ANR DEDALES under grant ANR-14-CE23-0005, Labex MME-DII, and the French Agency for Nuclear Waste Management (ANDRA). It also received funding from the European Research Council (ERC) under the European Union's Horizon 2020 research and innovation program (grant agreement No 647134 GATIPOR).

[†]Inria Paris, 2 rue Simone Iff, 75589 Paris, France & Université Paris-Est, CERMICS (ENPC), 77455 Marne-la-Vallée 2, France. elyes.ahmed@inria.fr, sarah.ali-hassan@inria.fr, michel.kern@inria.fr, martin.vohralik@inria.fr

[‡]Université Paris 13, Sorbonne Paris Cité, LAGA, CNRS (UMR 7539), 93430, Villetaneuse, France. japhet@math.univ-paris13.fr

because of the heterogeneity of the permeability, as well as the relative permeability and the capillary pressure that are functions of the saturation.

We consider in this paper a two-phase flow model introduced in [23] to study the phenomenon of oil or gas trapping in a porous medium with several rock types. This model, in which the convection is neglected, takes into account discontinuous capillary pressure functions across the interface between rock types. In particular, the existence of two different capillary pressure curves, discontinuous across the interface between the rock types, may play a role in preventing and isolating the radionuclide in the nuclear waste (see e.g. [46] and references therein). The effects of space-depending capillarities have been widely studied during the last years, see [23, 14, 16, 15, 12] for more details. The resulting problem is a nonlinear and degenerate parabolic equation for the saturation of the non-wetting phase, with nonlinear and discontinuous transmission conditions at the interface between the rocks. The numerical analysis of this problem has been considered in [23] for the model considered here, and in [12] for the full two-phase flow case. Existence of a weak solution was proved using the convergence of a finite volume scheme. In [14], Cancès proved the uniqueness of a weak solution for this model for a particular choice of functions characterizing the porous medium. In [16, 15], Cancès et al. proved the uniqueness of the full two-phase problem with convection terms in the one-dimensional case.

This model is formulated in [2] as a space-time transmission problem, which is solved with a non-overlapping space-time domain decomposition method. In the literature, few works exist for domain decomposition problems with jumping nonlinearities, although one can see for example [10, 11, 41] and the references therein. Domain decomposition methods for two phase flow problems were proposed in [50, 51], see also [29, 44, 45]. In such numerical approximations where the physics is quite complex, it is important to look at the quality of the resulting solution, as well as on the efficiency of the used algorithms. A practical tool is provided by a posteriori error estimates and adaptive stopping criteria for the different iterative methods involved in the calculation.

Some questions concerning a posteriori error estimates and stopping criteria in the context of Robin–Schwarz domain decomposition in combination with mixed finite element discretization for linear problems are treated in S. Ali Hassan's Ph.D. thesis [3], see also [4]. Previous contributions include [8, 6, 35, 25] for general techniques taking into account inexact algebraic solvers, [40] for multiscale mortar techniques in a unified treatment of various discretizations, [43, 42] for FETI and BDD algorithms combined with conforming finite element discretizations, and [19, 49, 17, 21] for a posteriori error estimates for two-phase flows, see also the reference therein. In these works, it is shown how a posteriori error estimates can distinguish between the various components of the error (space discretization, time discretization, domain decomposition, and the nonconformity error due to space-time domain decomposition with different time steps in the subdomains), thus leading to efficient stopping criteria for the (domain decomposition) iterations. To the best of our knowledge, contrarily to the case of linear problems, no results are available for a posteriori error estimates for the nonlinear problem with discontinuous transmission conditions.

The purpose of the present paper is threefold: first, to extend the work in [2] to a more general Schwarz method, with time-dependent Ventcell transmission conditions; second, to derive a posteriori error estimates for its finite volume–backward Euler approximation; and third, to address the question of when to stop the domain decomposition iterations as well as the iterations of the nonlinear solver used for the subdomain problems. With respect to the first point, our method is a space-time domain decomposition method based on optimized Schwarz waveform relaxation algorithm (OSWR) for solving time-dependent PDEs, in which at each OSWR iteration, space-time subdomain problems across the time interval are solved. The exchange between the subdomains is here ensured using time-dependent, higher-order transmission operators. Thus physically more valuable information is exchanged between the subdomains and hence a better convergence behavior can be expected (numerically observed in our experiments) for the resulting method, see [9, 13, 28, 30, 31, 33, 34, 38] and the references therein. All the derived results also naturally hold in the Robin case, obtained by setting one of the Ventcell parameters to zero. With respect to the second and third points, we build on the a posteriori methodology derived in [39, 47, 36, 24, 17, 22] for nonlinear, time-dependent problems, see also the references therein; we will in particular rely on [22, Theorem 5.2] for our error upper bound.

We measure the error between the unknown exact solution and the currently available approximate solution in energy-type norm introduced in [22]. At each iteration of the OSWR algorithm and on each linearization step, our estimates give a guaranteed and easily computable upper bound. This is achieved by introducing $\mathbf{H}(\mathrm{div})$-conforming and locally conservative flux reconstructions, piecewise constant in time,

following [24], and a saturation reconstruction, H^1-conforming in each subdomain, which is continuous and piecewise affine in time and satisfies the nonlinear discontinuous interface condition. The derived estimates are then splitted to the components corresponding to the space error, time error, linearization error, and the domain decomposition error. The benefits of such a procedure are to spare numerous iterations of the OSWR algorithm as well as of the linearization iterations used for the subdomain problems and to ensure tight overall error control at any point.

The outline of the paper is as follows: Section 2 recalls the physical model and defines weak solutions as well as the relevant functions spaces. Section 3 presents the space-time domain decomposition method with optimized Ventcell transmission conditions. In Section 4, we present the discrete OSWR algorithm, by combining a finite volume scheme for the discretization in the individual subdomains and the backward Euler time stepping with the OSWR method. We subsequently construct the needed ingredients for the a posteriori error estimates: Section 5 defines the postprocessing as well as the H^1-(subdomain by subdomain) and $\mathbf{H}(\mathrm{div})$-conforming reconstructions. Section 6 puts the pieces together by presenting a guaranteed and fully computable error estimate that bounds the energy-type error between the unknown exact solution and the approximate solution. In Section 7 we decompose this estimate into estimators characterizing the space, time, domain decomposition, and linearization error components. This is next used in Section 8 to propose stopping criteria for the OSWR algorithm and for the nonlinear iterations. The method is finally numerically validated on an example in three space dimensions in Section 9.

2 Presentation of the problem

Let Ω be an open bounded domain of $\mathbb{R}^d$ ($d = 2$ or 3) which is assumed to be polygonal if $d = 2$ and polyhedral if $d = 3$. We denote by $\partial\Omega$ its boundary (supposed to be Lipschitz-continuous) and by $\mathbf{n}$ the unit normal to $\partial\Omega$, outward to Ω. Let a time interval $(0, T)$ be given with $T > 0$. We consider a simplified model of a two-phase flow through a heterogeneous porous medium, in which the convection is neglected. Assuming that there are only two phases occupying the porous medium Ω, say gas and water, and that each phase is composed of a single component, the mathematical form of this problem as it is exposed in [23, 14] is as follows: given initial and boundary gas saturations u_0 and g, as well as a source term f, find $u : \Omega \times [0, T] \to [0, 1]$ such that

$$\partial_t u - \nabla\cdot(\lambda(u, \mathbf{x})\nabla\pi(u, \mathbf{x})) = f, \quad \text{in } \Omega \times (0, T), \tag{2.1a}$$

$$u(\cdot, 0) = u_0, \quad \text{in } \Omega, \tag{2.1b}$$

$$u = g, \quad \text{on } \partial\Omega \times (0, T). \tag{2.1c}$$

Here u is the gas saturation (and therefore $(1 - u)$ is the water saturation), $\pi(u, \mathbf{x}) : [0, 1] \times \Omega \to \mathbb{R}$ is the capillary pressure, and $\lambda(u, \mathbf{x}) : [0, 1] \times \Omega \to \mathbb{R}$ is the global mobility of the gas. For simplicity, we consider only Dirichlet boundary conditions on $\partial\Omega$. Other types of boundary conditions could be dealt with the same way as in [14, 23, 49]. The model problem given by (2.1a) is a nonlinear degenerate parabolic problem as the global mobility $\lambda(u) \to 0$ for $u \to 0$ and 1, and, moreover, $\pi'(u) \to 0$ for $u \to 0$ (see [7, 18]).

2.1 Flow between two rock types

In this part, we particularize the model problem (2.1a) to a porous medium with different capillary pressure curves π_i in each subdomain, following [23]. We suppose that Ω is composed of two disjoint subdomains Ω_i, $i = 1, 2$, which are both open polygonal subsets of $\mathbb{R}^d$ with Lipschitz-continuous boundary. We denote by Γ the interface between Ω_1 and Ω_2, i.e., $\Gamma = (\partial\Omega_1 \cap \partial\Omega_2)^\circ$. Let $\Gamma_i^{\mathrm{D}} = \partial\Omega_i \cap \partial\Omega$. Both data λ and π, which can in general depend on the physical characteristics of the rock, are henceforth supposed to be homogeneous in each subdomain Ω_i, $i = 1, 2$, i.e., $\lambda_i(\cdot) := \lambda_{|\Omega_i}(\cdot) = \lambda(\cdot, \mathbf{x}), \forall \mathbf{x} \in \Omega_i$, and similarly for π_i. The equations (2.1a) in each subdomain Ω_i then read as

$$\partial_t u_i - \nabla\cdot(\lambda_i(u_i)\nabla\pi_i(u_i)) = f_i, \quad \text{in } \Omega_i \times (0, T), \tag{2.2a}$$

$$u_i(\cdot, 0) = u_0, \quad \text{in } \Omega_i, \tag{2.2b}$$

$$u_i = g_i, \quad \text{on } \Gamma_i^{\mathrm{D}} \times (0, T). \tag{2.2c}$$

We use the notation $v_i = v|_{\Omega_i}$ for an arbitrary function v.

Before transcribing the transmission conditions on the interface Γ, we make precise the assumptions on the data (further generalizations are possible, bringing more technicalities):

Assumption 2.1 (Data). *1. For $i \in \{1,2\}$, $\pi_i \in C^1([0,1],\mathbb{R})$ can be extended in a continuous way to a function (still denoted by π_i) such that $\pi_i(u) = \pi_i(0)$ for all $u \leq 0$ and $\pi_i(u) = \pi_i(1)$ for all $u \geq 1$. Moreover, $\pi_i|_{[0,1]}$ is a strictly increasing function.*

2. For $i \in \{1,2\}$, $\lambda_i \in C^0([0,1],\mathbb{R}^+)$ is bounded and can be extended in a continuous way to a function (still denoted by λ_i) such that $\lambda_i(u) = \lambda_i(0)$ for all $u \leq 0$ and $\lambda_i(u) = \lambda_i(1)$ for all $u \geq 1$. We denote by C_λ an upper bound of $\lambda_i(u)$, $u \in \mathbb{R}$.

3. The initial condition is such that $u_0 \in L^\infty(\Omega)$ with $0 \leq u_0 \leq 1$ a.e. in Ω.

4. The boundary conditions $0 \leq g_i \leq 1$ are traces of some functions from $L^2(0,T;H^1(\Omega_i))$. For simplicity, we suppose them at most piecewise second-order polynomials with respect to the boundary faces of the spatial mesh introduced in Section 4.1.1 below, continuous on Γ_i^{D}, and constant in time. Moreover, they need to match in the sense that $\pi_1(g_1(\mathbf{x})) = \pi_2(g_2(\mathbf{x}))$ for all $\mathbf{x} \in \Gamma \cap \Gamma_1^{\mathrm{D}}$ and all $\mathbf{x} \in \Gamma \cap \Gamma_2^{\mathrm{D}}$.

5. The source term is such that $f \in L^2(0,T;L^2(\Omega))$. For simplicity we further assume that f is piecewise constant in time with respect to the temporal mesh introduced in Section 4.1.2 below.

We give now the transmission conditions needed to connect the subdomain problems (2.2), for $i = 1, 2$. We consider two cases. The first case is when

$$\pi_1(0) = \pi_2(0) \qquad \text{and} \qquad \pi_1(1) = \pi_2(1), \tag{2.3}$$

the same way as in [14]. If the functions π_i satisfy the above condition, the capillarity curves are said to be matching and the resulting transmission conditions on the interface are given by

$$\pi_1(u_1) = \pi_2(u_2), \qquad \text{on } \Gamma \times (0,T), \tag{2.4a}$$
$$\lambda_1(u_1)\nabla\pi_1(u_1)\cdot\mathbf{n}_1 = -\lambda_2(u_2)\nabla\pi_2(u_2)\cdot\mathbf{n}_2, \quad \text{on } \Gamma \times (0,T). \tag{2.4b}$$

These conditions yield a discontinuous saturation across the interface, i.e., we find that in general $u_1 \neq u_2$ on Γ.

In the second case, i.e., in the case when

$$\pi_1(0) \neq \pi_2(0) \qquad \text{or} \qquad \pi_1(1) \neq \pi_2(1), \tag{2.5}$$

the capillarity pressure curves are said to be non-matching. Consequently, not only the saturation is discontinuous at the medium interface, but also the capillary pressure field. The condition (2.5), studied in [23], has direct consequences on the behavior of the capillary pressures on both sides of the interface Γ. Indeed, suppose that $\pi_1(0) \leq \pi_2(0) < \pi_1(1) \leq \pi_2(1)$, and that u_1^* is the unique real in $[0,1]$ satisfying $\pi_1(u_1^*) = \pi_2(0)$, and u_2^* is the unique real in $[0,1]$ satisfying $\pi_2(u_2^*) = \pi_1(1)$. Then, if $u_1 \geq u_1^*$ and $u_2 \leq u_2^*$, we can still on the interface Γ prescribe the connection of the capillary pressures $\pi_1(u_1) = \pi_2(u_2)$ as in (2.4a). If $0 \leq u_1 \leq u_1^*$, the model imposes $u_2 = 0$, and the gas phase is entrapped in the rock Ω_1, and the water flows across Γ. In the same way, if $u_2^* \leq u_2 \leq 1$, the model prescribes $u_1 = 1$, and the water phase is captured in Ω_2 as a discontinuous phase, and the gas flows across Γ (see Figure 1 left). Following [23], these conditions on the gas-water saturations on the interface Γ are simply given by

$$\overline{\pi}_1(u_1) = \overline{\pi}_2(u_2), \qquad \text{on } \Gamma \times (0,T), \tag{2.6a}$$
$$\lambda_1(u_1)\nabla\pi_1(u_1)\cdot\mathbf{n}_1 = -\lambda_2(u_2)\nabla\pi_2(u_2)\cdot\mathbf{n}_2, \quad \text{on } \Gamma \times (0,T), \tag{2.6b}$$

where $\overline{\pi}_i$, for $i = 1, 2$, are truncated capillary pressure functions given on $[0,1]$ respectively by $\overline{\pi}_1 : u \mapsto \max(\pi_1(u), \pi_2(0))$ and $\overline{\pi}_2 : u \mapsto \min(\pi_2(u), \pi_1(1))$ (see Figure 1 right). In [23], it has been established that the model problem (2.2) together with the transmission conditions (2.6) has the necessary mathematical properties to explain the phenomena of gas trapping (see also [5, 16]).

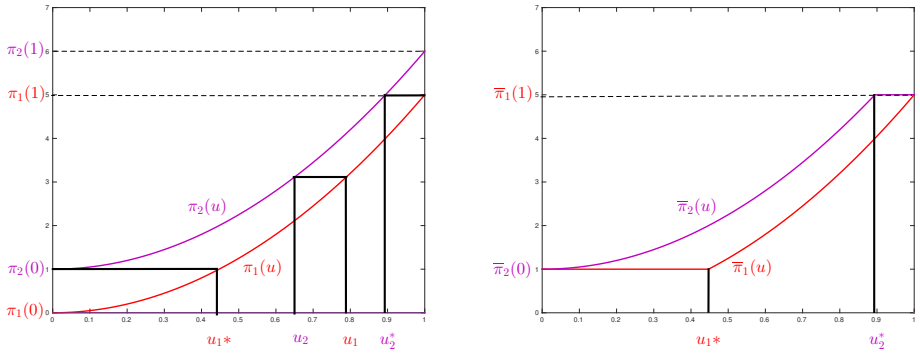

Figure 1: Capillary pressure curves (left) and truncated capillary pressures curves (right)

2.2 Transformation of the equations and weak formulation

Still following [23], we present here the mathematical quantities and function spaces used to characterize the weak solution to the multidomain problem (2.2) with the conditions (2.6). That of the problem (2.2) with the conditions (2.4) can be deduced straightforwardly from this later, see [14]. As Ω_i is a homogeneous rock type, so that π_i and λ_i do not depend on $\mathbf{x}$, one can define the Kirchhoff transform

$$\varphi_i : \left\{ \begin{array}{ccc} [0,1] & \longrightarrow & \mathbb{R}^+ \\ s & \longmapsto & \int_0^s \lambda_i(a)\pi_i'(a)\mathrm{d}a. \end{array} \right. \tag{2.7}$$

The function φ_i is Lipschitz-continuous and increasing on $[0,1]$, and we denote by $L_{\varphi,i}$ its Lipschitz constant, i.e., $L_{\varphi,i} := \max_{s\in[0,1]} \lambda_i(s)\pi_i'(s)$, so that

$$|\varphi_i(a) - \varphi_i(b)| \leq L_{\varphi,i}|a-b|, \quad \forall (a,b) \in [0,1]^2,$$

and we let $L_\varphi := \max(L_{\varphi,1}, L_{\varphi,2})$. We extend the function φ_i from $[0,1]$ to $\mathbb{R}$ so that $\varphi_i(u) = \varphi_i(0)$ for all $u \leq 0$ and $\varphi_i(u) = \varphi_i(1)$ for all $u \geq 1$.

We now introduce the strictly increasing function ϕ by

$$\phi : \left\{ \begin{array}{ccc} [\pi_2(0), \pi_1(1)] & \longrightarrow & \mathbb{R}^+ \\ s & \longmapsto & \displaystyle\int_{\pi_2(0)}^{s} \min_{j\in\{1,2\}} (\lambda_j \circ \pi_j^{-1}(a))\,\mathrm{d}a, \end{array} \right.$$

and let $\Pi_i := \phi \circ \overline{\pi}_i$, for $i \in \{1,2\}$. The functions $\Pi_i|_{[0,1]}$, introduced first in [23, Lemma 1.2] and used in [14, 16, 2], are differentiable and increasing. We let $\Pi_i(u) = \Pi_i(0)$ for all $u \leq 0$ and $\Pi_i(u) = \Pi_i(1)$ for all $u \geq 1$ and define the function Π by

$$\Pi(u, \mathbf{x}) = \Pi_i(u), \quad \text{for } \mathbf{x} \in \Omega_i.$$

As Π_i are more regular than $\overline{\pi}_i$, this allows to connect Π_1 and Π_2 instead of $\overline{\pi}_1$ and $\overline{\pi}_2$, that is, for all $(u_1, u_2) \in \mathbb{R}^2$, we have

$$\overline{\pi}_1(u_1) = \overline{\pi}_2(u_2) \Leftrightarrow \Pi_1(u_1) = \Pi_2(u_2).$$

Finally, under Assumption 2.1, the function $\Pi_i \circ \varphi_i^{-1}$ is Lipschitz-continuous with a Lipschitz constant lower than 1 (see [23]), i.e.

$$|\Pi_i(a) - \Pi_i(b)| \leq |\varphi_i(a) - \varphi_i(b)|, \quad \forall (a,b) \in [0,1]^2. \tag{2.8}$$

This inequality will be used in Remark 6.3 below.

We now apply the Kirchhoff transformation (2.7) separately in each subdomain, giving

$$\partial_t u_i - \Delta\varphi_i(u_i) = f_i, \qquad \text{in } \Omega_i \times (0,T), \tag{2.9a}$$
$$u_i(\cdot, 0) = u_0, \qquad \text{in } \Omega_i, \tag{2.9b}$$
$$\varphi_i(u_i) = \varphi_i(g_i), \quad \text{on } \Gamma_i^{\mathrm{D}} \times (0,T), \tag{2.9c}$$

together with the new expression of the conditions at the interface

$$\Pi_1(u_1) = \Pi_2(u_2), \qquad \text{on } \Gamma \times (0,T), \tag{2.10a}$$
$$\nabla\varphi_1(u_1)\cdot\mathbf{n}_1 = -\nabla\varphi_2(u_2)\cdot\mathbf{n}_2, \quad \text{on } \Gamma \times (0,T). \tag{2.10b}$$

Let us recall that some smoothness of the solutions u_i is required in order to ensure that the condition (2.10b) is well-defined on the interface Γ. In the general case, the multidomain problem (2.9)–(2.10) does not have any strong solution. This leads us to introduce the notion of a weak solution. To this aim, we define

$$X_{\varphi_i(g_i)} := L^2(0,T; H^1_{\varphi_i(g_i)}(\Omega_i)),$$
$$X_{\Pi(g,\cdot)} := L^2(0,T; H^1_{\Pi(g,\cdot)}(\Omega)), \qquad X := L^2(0,T; H^1_0(\Omega)),$$

where $H^1_{\varphi_i(g_i)}(\Omega_i) := \{v \in H^1(\Omega_i), v = \varphi_i(g_i) \text{ on } \Gamma_i^{\mathrm{D}}\}$ and similarly $H^1_{\Pi(g,\cdot)}(\Omega) := \{v \in H^1(\Omega), v = \Pi(g,\cdot) \text{ on } \partial\Omega\}$.

We equip the space X with the norm

$$||\psi||_X := \left\{ \int_0^T ||\nabla\psi(\cdot,t)||^2_{L^2(\Omega)} \,\mathrm{d}t \right\}^{\frac{1}{2}}.$$

The dual space of X is

$$X' := L^2(0,T; H^{-1}(\Omega)).$$

We will use the notation $\langle\cdot,\cdot\rangle_{H^{-1}(\Omega),H^1_0(\Omega)}$ to denote the duality pairing between $H^{-1}(\Omega)$ and $H^1_0(\Omega)$. We will also need the space

$$Z := H^1(0,T; H^{-1}(\Omega)).$$

We now define a weak solution to problem (2.9)–(2.10).

Definition 2.2 (Weak solution)**.** *We say that a function u is a weak solution to problem* (2.9)–(2.10) *if it satisfies:*

1. $u \in Z$;
2. $u(\cdot,0) = u_0$;
3. $\varphi_i(u_i) \in X_{\varphi_i(g_i)}$, *where* $u_i := u|_{\Omega_i}$, $i = 1,2$;
4. $\Pi(u,\cdot) \in X_{\Pi(g,\cdot)}$;
5. *For all $\psi \in X$, the following integral equality holds:*

$$\int_0^T \Big\{ \langle\partial_t u, \psi\rangle_{H^{-1}(\Omega),H^1_0(\Omega)} + \sum_{i=1}^{2} (\nabla\varphi_i(u_i), \nabla\psi)_{\Omega_i} - (f,\psi) \Big\} \mathrm{d}t = 0.$$

In this paper, we assume that a weak solution given by Definition 2.2 exists. One can then easily show that Π has sufficient regularity to impose the condition (2.10a). Indeed, since $\Pi_i \circ \varphi_i^{-1}$ is a Lipschitz-continuous function, the third point of Definition 2.2 ensures that $\Pi_i(u_i)$ belongs to $L^2(0,T; H^1(\Omega_i))$, $i = 1,2$. Thus, the point 4 of Definition 2.2 implies the continuity condition (2.10a). Finally, when supposing additionally that the weak solution u is sufficiently regular so that $\partial_t u \in L^2(0,T; L^2(\Omega))$, condition (2.10b) is satisfied weakly using point 5 of Definition 2.2.

Remark 2.3 (Existence and uniqueness of a weak solution)**.** *In [23], the existence of a weak solution to problem* (2.9)–(2.10) *(with homogeneous Neumann boundary conditions) was proved using integration by parts for the time term which requires a stronger test function space. Using the imposed conditions, one also finds $u \in L^\infty(0,T; L^\infty(\Omega))$, with $0 \le u \le 1$ a.e. in $\Omega \times (0,T)$. In fact, in [23] (see also [14]), the derived weak solution is given as the limit of a finite volume approximation of the solution refining the space and time discretization, and requires a stronger test function space for the application of the Kolmogorov's compactness criterion in L^∞. For the uniqueness, a first result was obtained in [14] for the case of matching capillary pressures curves. For the more general case, the uniqueness is demonstrated only for the one-dimensional case in [15].*

3 Space-Time Domain Decomposition Methods with Ventcell Transmission Conditions

Under sufficient regularity, an equivalent formulation to the model problem (2.9)–(2.10) can be obtained by solving, for $i = 1, 2$, equations (2.9) together with optimized Ventcell transmission conditions on $\Gamma \times (0, T)$

$$\nabla\varphi_1(u_1)\cdot\mathbf{n}_1 + \mathcal{L}_1(\Pi_1(u_1)) = -\nabla\varphi_2(u_2)\cdot\mathbf{n}_2 + \mathcal{L}_1(\Pi_2(u_2)), \tag{3.1a}$$
$$\nabla\varphi_2(u_2)\cdot\mathbf{n}_2 + \mathcal{L}_2(\Pi_2(u_2)) = -\nabla\varphi_1(u_1)\cdot\mathbf{n}_1 + \mathcal{L}_2(\Pi_1(u_1)), \tag{3.1b}$$

where $\mathcal{L}_i$, $i = 1, 2$, is a second-order (or Ventcell) boundary operator defined by

$$\mathcal{L}_i(v) := \alpha_{i,j}v + \gamma_{i,j}(\partial_t v - \Delta_\Gamma\, v), \quad j = (3 - i), \tag{3.2}$$

for a sufficiently regular function v defined on $\Gamma \times (0, T)$, where Δ_Γ represents the Laplace operator on Γ (Laplace–Beltrami operator). The Robin transmission conditions are easily obtained by taking in (3.2) the parameters $\gamma_{i,j} = 0$.

One can easily show that the operators $\mathcal{L}_i$ involve not only the continuity of the function Π as for the Robin case, but also the continuity of the time derivative and of the second-order derivatives of Π along the interface. As a result, this formulation can be seen as a coupling problem between a d-dimensional PDE in the rock Ω_i and a $(d-1)$-dimensional PDE on the interface Γ between the rock types, which greatly enhances the information exchange between the solutions in the subdomains, see [34, 28, 13, 31]. The Robin–Schwarz algorithm applied to this problem has been addressed in [2] and the existence of a weak solution of the local Robin problem (with $\gamma_{i,j} = 0$) in a multidimensional domain was obtained by proving the convergence of a finite volume scheme. Work underway addresses the Ventcell case using the same techniques. When the above multidomain problem is solved iteratively, the coefficients $\alpha_{i,j}$ and $\gamma_{i,j}$ can be chosen so as to minimize the convergence factor of the linearized algorithm as in [34, 28, 13, 31, 32, 33].

The Ventcell-OSWR algorithm is defined as follows: the solution u in the whole domain Ω given by $u_i = u|_{\Omega_i}$ is approximated by a sequence of solutions u_i^k, $k \geq 1$, defined recursively by

$$\partial_t u_i^k - \Delta\varphi_i(u_i^k) = f_i, \qquad \text{in } \Omega_i \times (0, T), \tag{3.3a}$$
$$u_i^k(\cdot, 0) = u_0, \qquad \text{in } \Omega_i, \tag{3.3b}$$
$$\varphi_i(u_i^k) = \varphi_i(g_i), \qquad \text{on } \Gamma_i^{\mathrm{D}} \times (0, T), \tag{3.3c}$$
$$\nabla\varphi_i(u_i^k)\cdot\mathbf{n}_i + \mathcal{L}_i(\Pi_i(u_i^k)) = \Psi_i^{k-1}, \qquad \text{on } \Gamma \times (0, T), \tag{3.3d}$$

with

$$\Psi_i^{k-1} := -\nabla\varphi_j(u_j^{k-1})\cdot\mathbf{n}_j + \mathcal{L}_i(\Pi_j(u_j^{k-1})), \quad j = (3 - i),\ k \geq 2, \tag{3.4}$$

and Ψ_i^0 is an initial Ventcell guess on $\Gamma \times (0, T)$.

Remark 3.1 (Interface operators)**.** *The multi-domain problem* (2.9) *together with the transmission conditions* (3.1) *can be formulated through the use of interface operators as a problem posed on the space-time interface, see [2], where Robin-to-Robin conditions are analyzed, and also [32, 33]. This interface problem can be solved iteratively by using fixed point iterations (which corresponds to the OSWR algorithm above) or via a Newton–Krylov method.*

4 The cell-centered finite volume scheme

We present in this section the OSWR algorithm (3.3)–(3.4) discretized by a finite volume method.

4.1 Space-time discretization, notations, and function spaces

We introduce here the partitions of Ω and Γ, time discretization, notation, and function spaces; see [26, 23, 24] for the standard part of the notation.

4.1.1 Partitions of Ω and Γ

Let $\mathcal{T}_{h,i}$ be a partition of the subdomain Ω_i into elements K, such that $\overline{\Omega_i} = \cup_{K\in\mathcal{T}_{h,i}} K$; here we suppose that they are either simplices or rectangular parallelepipeds but general elements can be treated via submeshes, see [21] and the references therein. Moreover, we assume that the partition is conforming in the sense that if K, $L \in \mathcal{T}_{h,i}$, $K \neq L$, then $K \cap L$ is either an empty set, a common face, edge, or vertex of K and L.

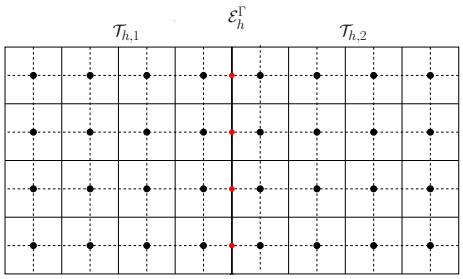

Figure 2: Compatible meshes in the subdomains in two space dimensions

We then set $\mathcal{T}_h = \cup_{i=1}^2 \mathcal{T}_{h,i}$ and denote by h the maximal element diameter in $\mathcal{T}_h$. The meshes are supposed to be matching on the interface Γ (see Figure 2). For all $K \in \mathcal{T}_h$, h_K denotes the diameter of the mesh element K and $|K|$ its volume. The interior mesh faces in $\mathcal{T}_{h,i}$ are collected into the set $\mathcal{E}_{h,i}^{\rm int}$, hence $\mathcal{E}_{h,i}^{\rm int}$ contains neither the subdomain interfaces nor the outer boundary of Ω. The faces of $\mathcal{T}_{h,i}$ lying on $\Gamma_i^{\rm D}$ are collected in the set $\mathcal{E}_{h,i}^{\rm D}$. We denote by $\mathcal{E}_{h,i}$ all the faces of $\mathcal{T}_{h,i}$ and we set $\mathcal{E}_h = \cup_{i=1}^2 \mathcal{E}_{h,i}$. The notation $\mathcal{E}_K$ stands for all the faces of an element $K \in \mathcal{T}_h$. Let $\mathcal{E}_h^\Gamma$ be a partition of Γ given by the faces of $\mathcal{T}_h$ on Γ. We use also $\mathcal{F}_{h,i}^{\rm int}$ to denote the interior sides (these are the points (if $d = 2$) or edges (if $d = 3$)) of $\mathcal{E}_h^\Gamma$. We denote by $\mathcal{F}_{h,i}^{\rm D}$ the sides of $\mathcal{E}_h^\Gamma$ on $\Gamma_i^{\rm D}$. The sides of a face $\sigma \in \mathcal{E}_h$ are collected in the set $\mathcal{F}_\sigma$. The volume of a face σ is denoted by $|\sigma|$ and that of a side e by $|e|$. Finally, we use the notation $\mathbf{x}_K$ to denote the "center" of the cell $K \in \mathcal{T}_h$. If $\sigma = K|L \in \mathcal{E}_h$ separates the cells K and L, $d_{K,L}$ denotes the Euclidean distance between $\mathbf{x}_K$ and $\mathbf{x}_L$, and $d_{K,\sigma}$ for $\sigma \in \mathcal{E}_K$ denotes the distance from $\mathbf{x}_K$ to σ. Similarly, we let $\mathbf{x}_\sigma$ be the "center" of the face σ and $\mathbf{x}_e$ the "center" of the edge e and denote respectively by $d_{\sigma,\tilde\sigma}$ and $d_{\sigma,e}$ the distance between $\mathbf{x}_\sigma$ and $\mathbf{x}_{\tilde\sigma}$ for $e = \sigma|\tilde\sigma \in \mathcal{F}_{h,i}^{\rm int}$ and the distance from $\mathbf{x}_\sigma$ to e for $e \in \mathcal{F}_\sigma$.

We assume that the composite mesh $\mathcal{T}_h$ satisfies the following orthogonality condition: for an interface $\sigma = K|L$, the line segment $\mathbf{x}_K\mathbf{x}_L$ is orthogonal to this interface (see [26]). The same condition should be satisfied for a side $e = \sigma|\tilde\sigma \in \mathcal{F}_{h,i}^{\rm int}$ due to the discretization of the Ventcell operator (see Figure 3).

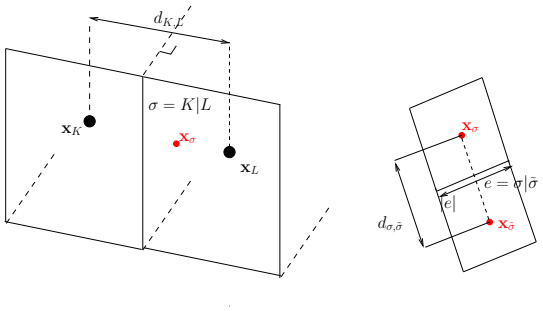

Figure 3: Notation for admissible meshes in three space dimensions

4.1.2 Time discretization

For an integer $N \geq 0$, let $(\tau^n)_{0\leq n\leq N}$ denote a sequence of positive real numbers corresponding to the discrete time steps such that $T = \sum_{n=1}^N \tau^n$. Let $t_0 = 0$, and $t^n = \sum_{j=1}^n \tau^j$, $1 \leq n \leq N$, be the discrete times. Let $I^n = (t^{n-1}, t^n]$, $1 \leq n \leq N$. For simplicity, we consider only conforming time grids. The analysis remains valid if we use different time steps in the subdomains, as was done in [3] for a linear diffusion problem.

4.1.3 Notation and function spaces

We denote by $\mathbb{P}_l(S)$ the space of polynomials on a subdomain $S \subset \Omega$ of total degree less than or equal to l and by

$$\mathbb{P}_l(\mathcal{T}_h) := \{p_h \in L^2(\Omega);\, p_h|_K \in \mathbb{P}_l(K),\ \forall K \in \mathcal{T}_h\},$$

the space of piecewise l-degree polynomials on $\mathcal{T}_h$. We use the notation $\|\cdot\|_K$ for the norm in $L^2(K)$, $K \in \mathcal{T}_h$. The corresponding inner product is $(\cdot,\cdot)_K$. We also denote by $(\cdot,\cdot)_\sigma$ the inner product in $L^2(\sigma)$ for $\sigma \in \mathcal{E}_h$. Let $|S|$ be the Lebesgue measure of S, and $|\sigma|$ the $(d-1)$-dimensional Lebesgue measure of $\sigma \in \mathbb{R}^{d-1}$. We define the broken Sobolev space $H^1(\mathcal{T}_h)$ as the space of all functions $v \in L^2(\Omega)$ such that $v|_K \in H^1(K)$, for all $K \in \mathcal{T}_h$. We will use the sign ∇ to denote the elementwise gradient, i.e., the gradient of a function restricted to a mesh element $K \in \mathcal{T}_h$. We define $P^1_\tau(H^1(\mathcal{T}_h))$ and $P^1_\tau(H^1_0(\Omega))$ as the space of continuous and piecewise affine in-time functions $v_{h\tau}$ with values in $H^1(\mathcal{T}_h)$ and in $H^1_0(\Omega)$, respectively. In both these situations, for every time step $1 \le n \le N$, we will use the abridged notation $v_h^n := v_{h\tau}(\cdot, t^n)$. By Assumption 2.1, the source function f is piecewise constant in time, i.e., constant on each time interval I^n, $1 \le n \le N$. Its value on I^n is denoted by $f^n := f|_{I^n}$.

The domain decomposition method we consider is global in time. Thus, at the space-time interface $\Gamma \times (0,T)$, data should be transferred from one space-time subdomain to the neighboring subdomain. Then, we denote by $P^0_\tau(L^2(\Gamma))$ the space of functions piecewise constant in time and with values in $L^2(\Gamma)$. Let $\mathbf{H}(\mathrm{div},\Omega)$ be the space of vector-valued functions from $\left[L^2(\Omega)\right]^d$ that admit a weak divergence $L^2(\Omega)$. Consequently, all functions in $\mathbf{H}(\mathrm{div},\Omega)$ have a continuous normal trace across the interface Γ. As above, $P^0_\tau(\mathbf{H}(\mathrm{div},\Omega))$ is the space of functions piecewise constant in time with values in $\mathbf{H}(\mathrm{div},\Omega)$. We use $\mathbf{RTN}_0(\Omega)$ to denote the lowest-order Raviart–Thomas–Nédélec finite-dimensional subspace of $\mathbf{H}(\mathrm{div},\Omega)$; any $\mathbf{v}_h \in \mathbf{RTN}_0(\Omega)$ takes on each element $K \in \mathcal{T}_h$ the form $[\mathbb{P}_0(K)]^d + \mathbb{P}_0(K)\mathbf{x}$ for the example of simplices.

Finally, given a function v that is double-valued on the interface Γ, the jump and the average of v on a face $\sigma \in \mathcal{E}_h^\Gamma$, $\sigma = K|L$, $K \in \mathcal{T}_{h,1}$, $L \in \mathcal{T}_{h,2}$, are defined as

$$[\![v]\!] = (v_K)\,|_\sigma - (v_L)\,|_\sigma, \qquad \{\!\{v\}\!\} = \frac{(v_K)\,|_\sigma + (v_L)\,|_\sigma}{2}.$$

Here $v_K = v|_K$ is the restriction of v to the element $K \in \mathcal{T}_h$.

4.2 A space-time fully discrete scheme based on finite volumes in space and the backward Euler scheme in time

Finite volume approximation is here not a piecewise constant function. For the iteration $k \ge 1$ of the OSWR algorithm, subdomain Ω_i, $i = 1, 2$, and the time steps $0 \le n \le N$, let the discrete saturation $u_{h,i}^{k,n} \in \mathbb{P}_0(\mathcal{T}_{h,i}) \times \mathbb{P}_0(\mathcal{E}_h^\Gamma)$ be identified with the vector of unknowns

$$u_{h,i}^{k,n} := \left((u_K^{k,n})_{K\in\mathcal{T}_{h,i}}, (u_{K,\sigma}^{k,n})_{\sigma\in\mathcal{E}_K\cap\mathcal{E}_h^\Gamma, K\in\mathcal{T}_{h,i}}\right).$$

Note that there are two interface unknowns for each face of $\mathcal{E}_h^\Gamma$.

We then define the discrete flux $F_{K,\sigma}$ over a face $\sigma \in \mathcal{E}_h \cap \mathcal{E}_K$, $K \in \mathcal{T}_{h,i}$, by

$$F_{K,\sigma}(u_{h,i}^{k,n}) := \begin{cases} \dfrac{\varphi_i(u_K^{k,n}) - \varphi_i(u_L^{k,n})}{d_{K,L}}, & \text{if } \sigma = K|L \in \mathcal{E}_{h,i}^{\mathrm{int}}, \\ \dfrac{\varphi_i(u_K^{k,n}) - \varphi_i(g_i(\mathbf{x}_\sigma))}{d_{K,\sigma}}, & \text{if } \sigma \in \mathcal{E}_K \cap \mathcal{E}_{h,i}^{\mathrm{D}}, \\ \dfrac{\varphi_i(u_K^{k,n}) - \varphi_i(u_{K,\sigma}^{k,n})}{d_{K,\sigma}}, & \text{if } \sigma \in \mathcal{E}_K \cap \mathcal{E}_h^\Gamma, \end{cases} \tag{4.1a}$$

and the discrete $(d-1)$-dimensional flux $\bar{F}_{\sigma,e}$ over a side $e \in \mathcal{F}_\sigma$, $\sigma \in \mathcal{E}_K \cap \mathcal{E}_h^\Gamma$, by

$$\bar{F}_{\sigma,e}(u_{h,i}^{k,n}) := \begin{cases} \dfrac{\Pi_i(u_{K,\sigma}^{k,n}) - \Pi_i(u_{K,\tilde{\sigma}}^{k,n})}{d_{\sigma,\tilde{\sigma}}}, & \text{if } e = \sigma|\tilde{\sigma} \in \mathcal{F}_\sigma \cap \mathcal{F}_{h,i}^{\mathrm{int}}, \\ \dfrac{\Pi_i(u_{K,\sigma}^{k,n}) - \Pi_i(g_i(\mathbf{x}_e))}{d_{\sigma,e}}, & \text{if } e \in \mathcal{F}_\sigma \cap \mathcal{F}_{h,i}^{\mathrm{D}}. \end{cases} \tag{4.1b}$$

Using (4.1), the finite volume approximation of the solution u^k in the OSWR algorithm (3.3)–(3.4) is: at each iteration $k \geq 1$, the initial condition is given by

$$u_K^{k,0} = \frac{1}{|K|}(u_0, 1)_K, \qquad \forall K \in \mathcal{T}_h, \tag{4.2a}$$

and for $n = 1, \ldots, N$, the discrete saturation $u_{h,i}^{k,n} \in \mathbb{P}_0(\mathcal{T}_{h,i}) \times \mathbb{P}_0(\mathcal{E}_h^\Gamma)$, $i = 1, 2$, is given by the following scheme:

$$\frac{u_K^{k,n} - u_K^{k,n-1}}{\tau^n}|K| + \sum_{\sigma \in \mathcal{E}_K} |\sigma| F_{K,\sigma}(u_{h,i}^{k,n}) = (f_i^n, 1)_K, \quad \forall K \in \mathcal{T}_{h,i}, \tag{4.2b}$$

$$-F_{K,\sigma}(u_{h,i}^{k,n}) + \gamma_{i,j}\frac{\Pi_i(u_{K,\sigma}^{k,n}) - \Pi_i(u_{K,\sigma}^{k,n-1})}{\tau^n}|\sigma| + \left(\Lambda_{K,\Gamma}(u_{h,i}^{k,n})\right)_\sigma = \Psi_{L,\sigma}^{k-1,n}, \quad \forall \sigma = K|L \in \mathcal{E}_h^\Gamma, \tag{4.2c}$$

where, for $K \in \mathcal{T}_{h,i}$,

$$\left(\Lambda_{K,\Gamma}(u_{h,i}^{k,n})\right)_\sigma := \alpha_{i,j}|\sigma|\Pi_i(u_{K,\sigma}^{k,n}) + \gamma_{i,j}\sum_{e \in \mathcal{F}_\sigma} |e| \bar{F}_{\sigma,e}(u_{h,i}^{k,n}), \quad \sigma \in \mathcal{E}_K \cap \mathcal{E}_h^\Gamma \tag{4.2d}$$

and, for $L \in \mathcal{T}_{h,j}$, $j = 3 - i$, and $\sigma = K|L \in \mathcal{E}_h^\Gamma$, the Ventcell information from Ω_j is

$$\Psi_{L,\sigma}^{k-1,n} := F_{L,\sigma}(u_{h,j}^{k-1,n}) + \gamma_{i,j}\frac{\Pi_j(u_{L,\sigma}^{k-1,n}) - \Pi_j(u_{L,\sigma}^{k-1,n-1})}{\tau^n}|\sigma| + \left(\Lambda_{L,\Gamma}(u_{h,j}^{k-1,n})\right)_\sigma. \tag{4.3}$$

4.3 Newton linearization

At each OSWR domain decomposition step $k \geq 1$ and each time step $n \geq 1$, the equations (4.2b)–(4.2c) constitute a block 2×2 system of nonlinear algebraic equations. Solving this system requires an iterative linearization procedure on each subdomain. We use for this purpose the Newton–Raphson method. We obtain at linearization step $m \geq 1$ the following scheme: find $u_{h,i}^{k,n,m} \in \mathbb{P}_0(\mathcal{T}_{h,i}) \times \mathbb{P}_0(\mathcal{E}_h^\Gamma)$, $u_{h,i}^{k,n,m} := \left((u_K^{k,n,m})_{K \in \mathcal{T}_{h,i}}, (u_{K,\sigma}^{k,n,m})_{\sigma \in \mathcal{E}_K \cap \mathcal{E}_h^\Gamma, K \in \mathcal{T}_{h,i}}\right)$, such that

$$\frac{u_K^{k,n,m} - u_K^{k,n-1}}{\tau^n}|K| + \sum_{\sigma \in \mathcal{E}_K} |\sigma| F_{K,\sigma}^{m-1}(u_{h,i}^{k,n,m}) = (f_i^n, 1)_K, \quad \forall K \in \mathcal{T}_{h,i}, \tag{4.4a}$$

$$-F_{K,\sigma}^{m-1}(u_{h,i}^{k,n,m}) + \gamma_{i,j}\frac{\Pi_i^{m-1}(u_{K,\sigma}^{k,n,m}) - \Pi_i(u_{K,\sigma}^{k,n-1})}{\tau^n}|\sigma| + \left(\Lambda_{K,\Gamma}^{m-1}(u_{h,i}^{k,n,m})\right)_\sigma = \Psi_{L,\sigma}^{k-1,n}, \quad \forall \sigma = K|L \in \mathcal{E}_h^\Gamma, \tag{4.4b}$$

where $F_{K,\sigma}^{m-1}(u_{h,i}^{k,n,m})$ are the linearized face fluxes given by

$$F_{K,\sigma}^{m-1}(u_{h,i}^{k,n,m}) := F_{K,\sigma}(u_{h,i}^{k,n,m-1}) + \sum_{M=K,L} \frac{\partial F_{K,\sigma}}{\partial u_M}(u_{h,i}^{k,n,m-1}) \cdot (u_M^{k,n,m} - u_M^{k,n,m-1}) + \frac{\partial F_{K,\sigma}}{\partial u_{K,\sigma}}(u_{h,i}^{k,n,m-1}) \cdot (u_{K,\sigma}^{k,n,m} - u_{K,\sigma}^{k,n,m-1}),$$

where the linearization of the function Π_i is

$$\Pi_i^{m-1}(u_{K,\sigma}^{k,n,m}) := \Pi_i(u_{K,\sigma}^{k,n,m-1}) + \frac{\partial \Pi_i}{\partial u_{K,\sigma}}(u_{K,\sigma}^{k,n,m-1})\cdot(u_{K,\sigma}^{k,n,m} - u_{K,\sigma}^{k,n,m-1}),$$

and where finally

$$\begin{aligned}\left(\Lambda_{K,\Gamma}^{m-1}(u_{h,i}^{k,n,m})\right)_\sigma := \left(\Lambda_{K,\Gamma}(u_{h,i}^{k,n,m-1})\right)_\sigma + \alpha_{i,j}|\sigma|\frac{\partial \Pi_i}{\partial u_{K,\sigma}}(u_{K,\sigma}^{k,n,m-1})\cdot(u_{K,\sigma}^{k,n,m} - u_{K,\sigma}^{k,n,m-1}) \\ + \gamma_{i,j}\sum_{e\in\mathcal{F}_\sigma}|e|\sum_{A=\sigma,\tilde{\sigma}}\frac{\partial \bar{F}_{\sigma,e}}{\partial u_A}(u_{h,i}^{k,n,m-1})\cdot(u_A^{k,n,m} - u_A^{k,n,m-1}).\end{aligned}$$

The equations (4.4a)–(4.4b) form a system of linear algebraic equations that is solved at each domain decomposition iteration k, at time step n, at each Newton iteration m and this independently in each of the subdomains Ω_i.

5 Postprocessing and H^1- and $\mathbf{H}(\mathrm{div})$-conforming reconstructions

At each OSWR iteration $k \geq 1$ and linearization step $m \geq 1$ of our method, let $u_{h\tau,i}^{k,m}$, $i = 1, 2$, be a piecewise constant in space and in time approximation given by the values $u_K^{k,n,m}$, $K \in \mathcal{T}_{h,i}$, $0 \leq n \leq N$. Thus also the approximate quantities $\varphi_i(u_{h\tau,i}^{k,m})$ and $\Pi_i(u_{h\tau,i}^{k,m})$, $i = 1, 2$, are piecewise constant. These approximations are not appropriate for an energy a posteriori error estimate. Following [48, 24, 40], our basic tools for the a posteriori error analysis will be:

(i) To construct a local postprocessing $\tilde{\varphi}_{h\tau,i}^{k,m}$ of $\varphi_i(u_{h\tau,i}^{k,m})$, $i = 1, 2$, using the known fluxes. This will be discontinuous piecewise quadratic in space and continuous piecewise affine in time. Therefrom, the postprocessed discontinuous saturation $\tilde{u}_{h,i}^{k,n,m}$ will be obtained by $\varphi_i^{-1}(\tilde{\varphi}_{h,i}^{k,n,m})$.

(ii) To construct from $\tilde{\varphi}_{h\tau,i}^{k,m}$ by averaging functions $\hat{\varphi}_{h\tau,i}^{k,m}$, piecewise quadratic in space and continuous in each Ω_i, and continuous piecewise affine in time. Therefrom, the reconstructed saturation $s_{h\tau}^{k,m}$ will be defined in the spirit of $\varphi_i^{-1}(\hat{\varphi}_{h,i}^{k,n,m})$; it will be continuous in each Ω_i and we will moreover ensure that $\Pi_1(s_{h\tau}^{k,m}|_{\Omega_1}) = \Pi_2(s_{h\tau}^{k,m}|_{\Omega_2})$ on the interface $\Gamma \times (0, T)$.

(iii) To construct a piecewise constant in-time and $\mathbf{RTN}_0(\Omega)$-conforming flux $\boldsymbol{\sigma}_{h\tau}^{k,m}$, locally conservative on the mesh $\mathcal{T}_h$.

5.1 Discontinuous piecewise quadratic $\tilde{\varphi}_{h,i}^{k,n,m}$ and postprocessed saturation $\tilde{u}_{h,i}^{k,n,m}$

Consider an OSWR iteration $k \geq 1$, a time step $1 \leq n \leq N$, and a linearization step $m \geq 1$. Let $\mathbf{u}_{h,i}^{k,n,m} \in \mathbf{RTN}_0(\Omega_i) \subset \mathbf{H}(\mathrm{div}, \Omega_i)$ be prescribed by the fluxes $F_{K,\sigma}(u_{h,i}^{k,n,m})$ in each subdomain Ω_i, $i = 1, 2$, i.e., on each $K \in \mathcal{T}_{h,i}$ and each face $\sigma \in \mathcal{E}_K$:

$$(\mathbf{u}_{h,i}^{k,n,m}\cdot\mathbf{n}_i, 1)_\sigma = (F_{K,\sigma}(u_{h,i}^{k,n,m}), 1)_\sigma. \tag{5.1}$$

Following [27, 48] and the references therein, we define the postprocessed approximation $\tilde{\varphi}_{h,i}^{k,n,m} \in \mathbb{P}_2(\mathcal{T}_{h,i})$ in each element $K \in \mathcal{T}_{h,i}$ as the solution of

$$-\nabla\tilde{\varphi}_{h,i}^{k,n,m}|_K = \mathbf{u}_{h,i}^{k,n,m}|_K, \quad \forall K \in \mathcal{T}_{h,i}, \tag{5.2a}$$

$$\frac{(\varphi^{-1}(\tilde{\varphi}_{h,i}^{k,n,m}), 1)_K}{|K|} = u_K^{k,n,m}, \quad \forall K \in \mathcal{T}_{h,i}. \tag{5.2b}$$

Remark 5.1 (Approximation)**.** *In practice, the condition* (5.2b) *will be approximated by a quadrature rule by* $\tilde{\varphi}_{h,i}^{k,n,m}(\mathbf{x}_K) = \varphi_i(u_K^{k,n,m})$ $\forall K \in \mathcal{T}_{h,i}$.

Procedure (5.2) is local in each element and its cost is negligible. The postprocessed approximation $\tilde{\varphi}_{h,i}^{k,n,m}$ is, however, not $H^1(\Omega_i)$-conforming, with jumps over the interior faces. We therefrom construct the corresponding postprocessed saturation by

$$\tilde{u}_{h,i}^{k,n,m} := \varphi_i^{-1}(\tilde{\varphi}_{h,i}^{k,n,m}). \tag{5.3}$$

Remark 5.2 (Practice)**.** *The postprocessed saturation $\tilde{u}_{h,i}^{k,n,m}$ will only be used for the theoretical analysis. In practice, the estimators in Theorem 6.1 below involving $\tilde{u}_{h,i}^{k,n,m}$ will be neglected and only the postprocessed $\tilde{\varphi}_{h,i}^{k,n,m}$ will be used to compute the error estimators. A practical approximate way to calculate the estimators involving $\tilde{u}_{h,i}^{k,n,m}$ is to use corresponding quadrature rules and to let* (5.3) *be satisfied at the quadrature nodes.*

We define the continuous, piecewise affine in-time functions $\tilde{u}_{h\tau,i}^{k,m}$ and $\tilde{\varphi}_{h\tau,i}^{k,m}$ by

$$\tilde{u}_{h\tau,i}^{k,m}(\cdot,t_n) = \tilde{u}_{h,i}^{k,n,m}, \qquad \tilde{\varphi}_{h\tau,i}^{k,m}(\cdot,t_n) = \tilde{\varphi}_{h,i}^{k,n,m}, \qquad 1 \le n \le N, \tag{5.4}$$

and define as usually $\tilde{u}_{h\tau}^{k,m}$ such that $\tilde{u}_{h\tau}^{k,m}|_{\Omega_i} := \tilde{u}_{h\tau,i}^{k,m}$.

5.2 Continuous piecewise quadratic $\hat{\varphi}_{h,i}^{k,n,m}$ and H^1-conforming reconstruction $s_{h\tau}^{k,m}$

Consider an OSWR iteration $k \ge 1$ and a linearization step $m \ge 1$. In this section, we define a reconstructed saturation such that

$$s_{h\tau}^{k,m} \in Z, \qquad \varphi_i(s_{h\tau,i}^{k,m}) \in X_{\varphi_i(g_i)},\ i=1,2, \qquad \Pi(s_{h\tau}^{k,m},\cdot) \in X_{\Pi(g,\cdot)},$$

reflecting the properties of the weak solution u of Definition 2.2. Practically, we in particular require that, at each time step $1 \le n \le N$,

$$s_h^{k,n,m}|_{\Gamma_i^{\mathrm{D}}} = g_i \text{ on } \Gamma_i^{\mathrm{D}},\ i=1,2, \tag{5.5a}$$

$$\Pi_1(s_h^{k,n,m}|_{\Omega_1}) = \Pi_2(s_h^{k,n,m}|_{\Omega_2}) \text{ on } \Gamma, \tag{5.5b}$$

$$\frac{1}{|K|}(s_h^{k,n,m},1)_K = u_K^{k,n,m}, \quad \forall K \in \mathcal{T}_h, \tag{5.5c}$$

where the technical requirement (5.5c) will be easy to satisfy using the bubble functions following [24]. Then the continuous piecewise affine in-time function $s_{h\tau}^{k,m}$ is prescribed by

$$s_{h\tau}^{k,m}(\cdot,t_n) = s_h^{k,n,m}, \qquad 1 \le n \le N. \tag{5.6}$$

As usually, $s_{h\tau,i}^{k,m} := s_{h\tau}^{k,m}|_{\Omega_i}$.

5.2.1 Continuous piecewise quadratic $\hat{\varphi}_{h,i}^{k,n,m}$

For a given postprocessed function $\tilde{\varphi}_{h,i}^{k,n,m} \in \mathbb{P}_2(\mathcal{T}_{h,i})$ defined by (5.2), we now prescribe at the degrees of freedom of $\mathbb{P}_2(\mathcal{T}_{h,i}) \cap H^1(\Omega_i)$ a piecewise continuous polynomial $\hat{\varphi}_{h,i}^{k,n,m} \in \mathbb{P}_2(\mathcal{T}_{h,i}) \cap H^1(\Omega_i)$. If $\mathbf{x}$ is a Lagrange node situated in the interior of Ω_i or at the interface Γ, we set

$$\hat{\varphi}_{h,i}^{k,n,m}(\mathbf{x}) := \mathcal{I}_{\mathrm{av}}(\tilde{\varphi}_{h,i}^{k,n,m})(\mathbf{x}),$$

where $\mathcal{I}_{\mathrm{av}} : \mathbb{P}_2(\mathcal{T}_{h,i}) \to \mathbb{P}_2(\mathcal{T}_{h,i}) \cap H^1(\Omega_i)$ is the interpolation operator given by

$$\mathcal{I}_{\mathrm{av}}(\phi_h)(\mathbf{x}) = \frac{1}{|\mathcal{T}_{\mathbf{x}}|} \sum_{K \in \mathcal{T}_{\mathbf{x}}} \phi_h|_K(\mathbf{x}),$$

with $\mathcal{T}_{\mathbf{x}}$ the set of all the elements of $\mathcal{T}_{h,i}$ sharing the node $\mathbf{x}$. At the Lagrange nodes $\mathbf{x}$ situated on the boundary Γ_i^{D}, we set $\hat{\varphi}_{h,i}^{k,n,m}(\mathbf{x}) := \varphi_i(g_i(\mathbf{x}))$.

5.2.2 H^1-conforming reconstruction $s_{h\tau}^{k,m}$

We now consider $\varphi_i^{-1}(\hat{\varphi}_{h,i}^{k,n,m})$ and modify them at the interface Γ in order to satisfy (5.5b), as well as on the boundaries Γ_i^{D} to satisfy (5.5a). In order to satisfy the mean value condition (5.5c), we proceed as in [24, Section 3.2.2] and employ the bubble functions b_K over each element $K \in \mathcal{T}_h$ (the product of the barycentric coordinates for a simplex), multiplied by suitable constants α_K.

Remark 5.3 (Practice)**.** *In practice, one can only satisfy condition* (5.5b) *in the sense of quadrature. Indeed, for $1 \le n \le N$, $1 \le i \le 2$, and any node $\mathbf{x}_\Gamma$ of the chosen quadrature rule lying at the interface Γ, we can request*

$$\Pi_i(s_h^{k,n,m}|_{\Omega_i}(\mathbf{x}_\Gamma)) = \frac{\Pi_i(\varphi_i^{-1}(\hat{\varphi}_{h,i}^{k,n,m}(\mathbf{x}_\Gamma))) + \Pi_j(\varphi_j^{-1}(\hat{\varphi}_{h,j}^{k,n,m}(\mathbf{x}_\Gamma)))}{2}.$$

Similarly, equation (5.5c) *will also typically only be satisfied up to a quadrature error.*

5.3 Equilibrated flux reconstruction $\boldsymbol{\sigma}_{h\tau}^{k,m}$

Because of the domain decomposition formulation with Robin or Ventcell transmission conditions, the finite volume fluxes $F_{K,\sigma}(u_{h,i}^{k,n,m})$ (or their linearizations $F_{K,\sigma}^{m-1}(u_{h,i}^{k,n,m})$) do not match from the two sides of the interface Γ. Consequently, $\mathbf{u}_h^{k,n,m}$ given by (5.1) is not $\mathbf{H}(\mathrm{div},\Omega)$-conforming, i.e., it does not lie in the space $\mathbf{RTN}_0(\Omega)$. We now present, following [3], a procedure allowing to construct an equilibrated flux $\boldsymbol{\sigma}_{h\tau}^{k,m}$ that satisfies

$$\boldsymbol{\sigma}_{h\tau}^{k,m} \in P_\tau^0(\mathbf{RTN}_0(\Omega)), \tag{5.7a}$$

$$\left(f^n - \frac{u_K^{k,n,m} - u_K^{k,n-1}}{\tau^n} - \nabla\cdot\boldsymbol{\sigma}_h^{k,n,m}, 1\right)_K = 0, \quad \forall K \in \mathcal{T}_h. \tag{5.7b}$$

For each subdomain Ω_i, we consider a subset B_i of Ω_i, termed a band, which contains all the elements of $\mathcal{T}_{h,i}$ that share a face with the interface Γ. We denote by $\mathcal{T}_{h,i}^B$ the resulting submesh. We start by setting

$$\boldsymbol{\sigma}_h^{k,n,m}|_K := \mathbf{u}_h^{k,n,m}|_K, \quad \forall K \in \mathcal{T}_{h,i} \text{ s.t. } K \subset \Omega_i \backslash B_i. \tag{5.8}$$

In the bands, we will modify $\mathbf{u}_h^{k,n,m}$ so as to arrive at (5.7); note that simply prescribing the normal components of $\boldsymbol{\sigma}_h^{k,n,m}$ by $\{\!\{\mathbf{u}_{h,i}^{k,n,m}\cdot\mathbf{n}_{B_i}\}\!\}$ at the interface would lead to (5.7a) but not to (5.7b).

We first calculate the mass balance misfit by

$$err_i^{k,n,m} = \left(f_i^n - \frac{u_K^{k,n,m} - u_K^{k,n-1}}{\tau^n}, 1\right)_{B_i} - (\{\!\{\mathbf{u}_{h,i}^{k,n,m}\cdot\mathbf{n}_{B_i}\}\!\}, 1)_{\partial B_i}, \quad i = 1,2,$$

where $\mathbf{n}_{B_i}$ is the outward unit vector normal to ∂B_i. We next denote by Γ_i^b, $b = 1,2,3,4$, the four boundaries (in 3D) of ∂B_i that intersect $\partial\Omega$, for $i = 1,2$. We denote also by Γ_i^{int} the boundary of ∂B_i that is inside Ω_i, $i = 1,2$, see Figure 4. We then identify nine corrections $\left(c_{\Gamma_1^b}^{k,n,m}\right)_{1\le b\le 4}$, $\left(c_{\Gamma_2^b}^{k,n,m}\right)_{1\le b\le 4}$, and $c_\Gamma^{k,n,m}$ to the averaged flux $\{\!\{\mathbf{u}_{h,i}^{k,n,m}\cdot\mathbf{n}_{B_i}\}\!\}$ that will lead to equilibrium in each band B_i, $i = 1,2$. In other words, we seek to satisfy the two balancing conditions:

$$\sum_{b=1}^{4} c_{\Gamma_i^b}^{k,n,m} + (\mathbf{n}_\Gamma\cdot\mathbf{n}_{B_i})c_\Gamma^{k,n,m} = err_i^{k,n,m}, \quad i = 1,2. \tag{5.9}$$

Here $\mathbf{n}_\Gamma$ is a unit vector normal to Γ, pointing either from Ω_1 to Ω_2, or from Ω_2 to Ω_1.

The interface problem (5.9) is a rectangular linear system of nine unknowns and two equations and is solved via the least squares minimization; it may be seen as a coarse-grid balancing solve in a simplified version of [20], tailored to Robin or Ventcell boundary conditions. Finally, the corrections are distributed from the boundary of the bands to their interiors by approximating, using the mixed finite element or the

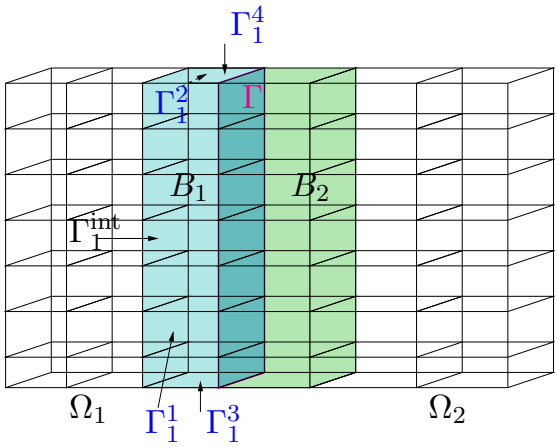

Figure 4: Bands B_1 and B_2 surrounding the interface Γ in three space dimensions

finite volume method, the following local Neumann problems: find $(q_{h,i}^{k,n,m}, \boldsymbol{\sigma}_{h,i}^{k,n,m}) \in \mathbb{P}_0(\mathcal{T}_{h,i}^B) \times \mathbf{RTN}_0(B_i)$ with $(q_{h,i}^{k,n,m}, 1)_{B_i} = 0$ such that

$$\begin{cases} \nabla\cdot\boldsymbol{\sigma}_{h,B_i}^{k,n,m}|_K = f_i^n|_K - \dfrac{u_K^{k,n,m} - u_K^{k,n-1,m}}{\tau^n} & \forall K \in \mathcal{T}_{h,i}^B, \\ \boldsymbol{\sigma}_{h,B_i}^{k,n,m} - \mathbf{u}_{h,i}^{k,n,m} = -\nabla q_{h,i}^{k,n,m}, & \text{in } B_i, \\ \boldsymbol{\sigma}_{h,B_i}^{k,n,m}\cdot\mathbf{n}_\Gamma = \mathbf{u}_{h,i}^{k,n,m}\cdot\mathbf{n}_\Gamma, & \text{on } \Gamma_i^{\text{int}}, \\ \boldsymbol{\sigma}_{h,B_i}^{k,n,m}\cdot\mathbf{n}_\Gamma = \{\!\{\mathbf{u}_h^{k,n,m}\cdot\mathbf{n}_\Gamma\}\!\} + \dfrac{1}{|\Gamma|}c_\Gamma^{k,n,m}, & \text{on } \Gamma, \\ \boldsymbol{\sigma}_{h,B_i}^{k,n,m}\cdot\mathbf{n}_\Gamma = \mathbf{u}_{h,i}^{k,n,m}\cdot\mathbf{n}_\Gamma + \dfrac{1}{|\Gamma_i^b|}c_{\Gamma_i^b}^{k,n,m}, & \text{on } \Gamma_i^b. \end{cases}$$

We finally complement (5.8) by setting $\boldsymbol{\sigma}_h^{k,n,m}|_{B_i} := \boldsymbol{\sigma}_{h,B_i}^{k,n,m}$.

6 A posteriori error estimate

Relying on the developments of the previous sections, we derive here a posteriori error estimates that include the domain decomposition error. More precisely, at each OSWR iteration $k \geq 1$ and at each linearization step $m \geq 1$, we bound an energy error between the postprocessed saturation $\tilde{u}_{h\tau}^{k,m}$ defined in Section 5.1 and the weak solution u of Definition 2.2 by a guaranteed and fully computable upper bound. Before formulating the a posteriori error estimates, we recall the Poincaré inequality:

$$\|q - q_K\| \leq C_{\mathrm{P},K} h_K \|\nabla q\|_K, \quad \forall q \in H^1(K),$$

where q_K is the mean value of the function q on the element K and $C_{\mathrm{P},K} = 1/\pi$ whenever the element K is convex.

It is important to stress that the result below applies to all functions $s_{h\tau}^{k,m} \in Z$, such that $\varphi_i(s_{h\tau,i}^{k,m}) \in X_{\varphi_i(g_i)}$ and $\Pi(s_{h\tau}^{k,m}, \cdot) \in X_{\Pi(g,\cdot)}$. For all times $t \in (0,T)$, let

$$Q_{t,i} := L^2(0,t;L^2(\Omega_i)), \qquad X_t := L^2(0,t;H_0^1(\Omega)), \qquad X_t' := L^2(0,t;H^{-1}(\Omega)).$$

Because of the assumptions on the weak solution u in Definition 2.2 and since $\varphi_i(\tilde{u}_{h\tau,i}^{k,m}) = \tilde{\varphi}_{h\tau,i}^{k,m} \in L^2(0,T;L^2(\Omega_i))$ by (5.3)–(5.4), $\tilde{u}_{h\tau}^{k,m} \in X'$, and $\tilde{u}_{h\tau}^{k,m}(\cdot,T) \in H^{-1}(\Omega)$, we can define two energy-type error

measures, following [22], as

$$\|u-\tilde{u}_{h\tau}^{k,m}\|_\star^2 := \sum_{i=1}^{2}\|\varphi_i(u_i)-\varphi_i(\tilde{u}_{h\tau,i}^{k,m})\|_{Q_{T,i}}^2+\frac{L_\varphi}{2}\|u-\tilde{u}_{h\tau}^{k,m}\|_{X'}^2 +\frac{L_\varphi}{2}\|(u-\tilde{u}_{h\tau}^{k,m})(\cdot,T)\|_{H^{-1}(\Omega)}^2 \tag{6.1}$$

and

$$\|u-\tilde{u}_{h\tau}^{k,m}\|_\sharp^2 := \|u-\tilde{u}_{h\tau}^{k,m}\|_\star^2 + 2\sum_{i=1}^{2}\int_0^T\left(\|\varphi_i(u_i)-\varphi_i(\tilde{u}_{h\tau,i}^{k,m})\|_{Q_{t,i}}^2+\int_0^t\|\varphi_i(u_i)-\varphi_i(\tilde{u}_{h\tau,i}^{k,m})\|_{Q_{s,i}}^2e^{t-s}\mathrm{d}s\right)\mathrm{d}t; \tag{6.2}$$

recall that L_φ is the maximal Lipschitz constant of the functions φ_i defined by (2.7). We will also need the weaker distance

$$\|u-s_{h\tau}^{k,m}\|_\flat := \sqrt{\frac{L_\varphi}{2}}\Bigg\{(2e^T-1)\|u_0-s_{h\tau}^{k,m}(\cdot,0)\|_{H^{-1}(\Omega)}^2+\|\mathcal{R}(s_{h\tau}^{k,m})\|_{X'}^2 +2\int_0^T\Big(\|\mathcal{R}(s_{h\tau}^{k,m})\|_{X_t'}^2+\int_0^t\|\mathcal{R}(s_{h\tau}^{k,m})\|_{X_s'}^2e^{t-s}\mathrm{d}s\Big)\mathrm{d}t\Bigg\}^{\frac12} \tag{6.3}$$

featuring the residual $\mathcal{R}(s_{h\tau}^{k,m})$ of $s_{h\tau}^{k,m}$, given for $\psi\in X$, by

$$\begin{aligned}&\langle\mathcal{R}(s_{h\tau}^{k,m}),\psi\rangle_{X',X}\\ &:=\int_0^T\Big\{(f,\psi)-\langle\partial_t s_{h\tau}^{k,m},\psi\rangle_{H^{-1}(\Omega),H_0^1(\Omega)}-\sum_{i=1}^{2}(\nabla\varphi_i(s_{h\tau,i}^{k,m}),\nabla\psi)_{\Omega_i}\Big\}(s)\mathrm{d}s,\end{aligned}$$

and its dual norm given by

$$\|\mathcal{R}(s_{h\tau}^{k,m})\|_{X'} := \sup_{\psi\in X,\,\|\psi\|_X=1}\langle\mathcal{R}(s_{h\tau}^{k,m}),\psi\rangle_{X',X}.$$

Our main result is summarized in the following theorem:

Theorem 6.1 (A posteriori error estimate)**.** *Let u be the weak solution of the multidomain problem* (2.9)–(2.10) *in the sense of Definition 2.2. Let $\tilde{u}_{h\tau}^{k,m}$ be the postprocessed saturation at the iteration $k\geq1$ and the linearization step $m\geq1$, prescribed by* (5.3)–(5.4) *from the linearized finite volume OSWR scheme of Section 4.3. Let $s_{h\tau}^{k,m}$ and $\boldsymbol{\sigma}_{h\tau}^{k,m}$ be the reconstructed functions as obtained in Sections 5.2 and 5.3. Then*

$$\|u-s_{h\tau}^{k,m}\|_\flat\leq\eta^{k,m}. \tag{6.4}$$

Moreover, if

$$\bar{\varphi}\in X,\quad \textit{where}\quad \bar{\varphi}|_{\Omega_i}:=\varphi_i(u_i)-\varphi_i(s_{h\tau,i}^{k,m}),\quad i=1,2, \tag{6.5}$$

then

$$\|u-\tilde{u}_{h\tau}^{k,m}\|_\sharp\leq\eta^{k,m}+\|\tilde{u}_{h\tau}^{k,m}-s_{h\tau}^{k,m}\|_\sharp. \tag{6.6}$$

Here

$$\eta^{k,m} := \sqrt{\frac{L_\varphi}{2}}\Bigg\{(2e^T-1)\big(\eta_{\mathrm{IC}}^{k,m}\big)^2+\sum_{n=1}^{N}\big(\eta^{k,n,m}\big)^2 +2\sum_{n=1}^{N}\tau^n\sum_{l=1}^{n}\big(\eta^{k,l,m}\big)^2+2\sum_{n=1}^{N}\sum_{l=1}^{n}J_{nl}\Big(\sum_{q=1}^{l}\big(\eta^{k,q,m}\big)^2\Big)\Bigg\}^{\frac12}, \tag{6.7a}$$

the initial condition estimator $\eta_{\mathrm{IC}}^{k,m}$ *and the estimators* $\eta^{k,n,m}$ *are respectively defined by*

$$\eta_{\mathrm{IC}}^{k,m} := \|u_0 - s_{h\tau}^{k,m}(\cdot,0)\|_{H^{-1}(\Omega)}, \tag{6.7b}$$

$$\eta^{k,n,m} := \left\{ \int_{I^n} \sum_{i=1}^{2} \sum_{K\in\mathcal{T}_{h,i}} \left(\eta_{\mathrm{R},K}^{k,n,m} + \eta_{\mathrm{disc},K,i}^{k,n,m}(t) \right)^2 \mathrm{d}t \right\}^{\frac{1}{2}}, \quad 1 \le n \le N, \tag{6.7c}$$

with the residual and the discretization estimators given respectively by

$$\eta_{\mathrm{R},K}^{k,n,m} := C_{\mathrm{P},K} h_K \|f^n - \partial_t s_{h\tau}^{k,m} - \nabla\cdot\boldsymbol{\sigma}_h^{k,n,m}\|_K, \quad K \in \mathcal{T}_h, \tag{6.7d}$$

$$\eta_{\mathrm{disc},K,i}^{k,n,m}(t) := \|\boldsymbol{\sigma}_h^{k,n,m} + \nabla\varphi_i(s_{h\tau}^{k,m}(\cdot,t))\|_K, \quad K \in \mathcal{T}_{h,i},\ t \in I^n, \tag{6.7e}$$

and where we have set, for $1 \le n, l \le N$,

$$J_{nl} := \int_{I^n}\int_{I^l} e^{t-s}\mathrm{d}s\mathrm{d}t.$$

Proof. We have set $s_{h\tau}^{k,m}$ so that $\varphi_i(s_{h\tau,i}^{k,m}) \in X_{\varphi_i(g_i)}$, $\Pi(s_{h\tau}^{k,m},\cdot) \in X_{\Pi(g,\cdot)}$, and

$$(f^n - \partial_t s_{h\tau}^{k,m}|_{I^n} - \nabla\cdot\boldsymbol{\sigma}_h^{k,n,m}, 1)_K = 0 \qquad \forall K \in \mathcal{T}_h,\ 1 \le n \le N. \tag{6.8}$$

Indeed, (6.8) follows from (5.7b) and from the requirement (5.5c) as in [24, Lemma 3.1]. Thus we can proceed as in [22, Theorem 5.3] to see (6.4). Next, it follows by inspection of the proof of [22, Theorem 5.2] that, under assumption (6.5), we have

$$\|u - s_{h\tau}^{k,m}\|_\sharp \le \|u - s_{h\tau}^{k,m}\|_\flat. \tag{6.9}$$

Thus, (6.6) follows by the triangle inequality

$$\|u - \tilde{u}_{h\tau}^{k,m}\|_\sharp \le \|u - s_{h\tau}^{k,m}\|_\sharp + \|\tilde{u}_{h\tau}^{k,m} - s_{h\tau}^{k,m}\|_\sharp.$$

□

Remark 6.2 (Condition (6.5))**.** *Condition* (6.5) *seems unfortunately necessary to apply [22, Theorem 5.2] so as to obtain* (6.9) *and consequently the a posteriori estimate* (6.6) *in the norm* $\|\cdot\|_\sharp$*. It is indeed rather restrictive for the complete problem* (2.9)–(2.10)*. It is, though, in particular satisfied when the global mobilities of the gas* λ_i *are constants in the respective subdomains* Ω_i *and* $\pi_1(0) = \pi_2(0)$*.*

Remark 6.3 (A posteriori estimate of the saturation and capillary pressure errors)**.** *Applying* (2.8)*, the above estimators bound also the saturation and the capillary pressure errors. More precisely, replacing the functions* φ_i *by the functions* Π_i *everywhere in* (6.1)–(6.2)*, the estimate* (6.6) *still holds.*

7 An a posteriori error estimate distinguishing the space, time, linearization, and the DD errors

In this section, we distinguish the different error components, proceeding as in [25, 17, 22, 3] and the references therein. The aim is in particular to separate the domain decomposition error from the estimated space, time, and linearization errors.

For the iteration $k \ge 1$ of the OSWR algorithm, for all time steps $0 \le n \le N$, a linearization step $m \ge 1$, and both subdomains Ω_i, $i = 1, 2$, we define a vector function $\boldsymbol{\ell}_{h,i}^{k,n,m} \in \mathbf{RTN}(\Omega_i)$ that approximates the available flux used in the Newton iterations in Section 4.3, i.e.,

$$(\boldsymbol{\ell}_{h,i}^{k,n,m}\cdot\mathbf{n}_i, 1)_\sigma = (F_{K,\sigma}^{m-1}(u_{h,i}^{k,n,m}), 1)_\sigma, \quad \forall\sigma \in \mathcal{E}_K,\ \forall K \in \mathcal{T}_{h,i}. \tag{7.1}$$

The vector function $\boldsymbol{\ell}_{h,i}^{k,n,m}$ is called the linearized flux. It tends to $\mathbf{u}_{h,i}^{k,n,m}$ defined in (5.1) at convergence of the Newton algorithm. For all $K \in \mathcal{T}_{h,i}$, we then define the local *spatial*, *temporal*, *domain decomposition*, and *linearization* estimators by:

$$\eta_{\mathrm{sp},K,i}^{k,n,m} := \eta_{\mathrm{R},K}^{k,n,m} + \|\nabla\varphi_i(s_{h\tau}^{k,m}(\cdot,t_n)) + \boldsymbol{\ell}_{h,i}^{k,n,m}\|_K, \tag{7.2a}$$

$$\eta_{\mathrm{tm},K,i}^{k,n,m}(t) := \|\nabla\big(\varphi_i(s_{h\tau}^{k,m}(\cdot,t)) - \varphi_i(s_{h\tau}^{k,m}(\cdot,t_n))\big)\|_K, \tag{7.2b}$$

$$\eta_{\mathrm{dd},K,i}^{k,n,m} := \|\nabla\varphi_i(\tilde{u}_{h,i}^{k,n,m}) + \boldsymbol{\sigma}_h^{k,n,m}\|_K, \tag{7.2c}$$

$$\eta_{\mathrm{lin},K,i}^{k,n,m} := \|\nabla\varphi_i(\tilde{u}_{h,i}^{k,n,m}) + \boldsymbol{\ell}_{h,i}^{k,n,m}\|_K; \tag{7.2d}$$

note that from (5.3) and (5.2a), $-\nabla\varphi_i(\tilde{u}_{h,i}^{k,n,m}) = \mathbf{u}_{h,i}^{k,n,m}$, so that (7.2c) and (7.2d) only work with lowest-order Raviart–Thomas–Nédélec polynomials, so that they can be evaluated without numerical quadrature error and fast. Set, like in (6.7c), for $\mathrm{a} = \mathrm{sp}, \mathrm{tm}, \mathrm{dd}, \mathrm{lin}$,

$$\big(\eta_{\mathrm{a},i}^{k,n,m}\big)^2 := \int_{I^n} \sum_{K\in\mathcal{T}_{h,i}} \big(\eta_{\mathrm{a},K,i}^{k,n,m}\big)^2 \mathrm{d}t \quad \text{and} \quad \big(\eta_{\mathrm{a}}^{k,n,m}\big)^2 := \sum_{i=1}^{2} \big(\eta_{\mathrm{a},i}^{k,n,m}\big)^2, \tag{7.3}$$

and note that except for $\mathrm{a} = \mathrm{tm}$, $\big(\eta_{\mathrm{a},i}^{k,n,m}\big)^2 = \tau^n \sum_{K\in\mathcal{T}_{h,i}} \big(\eta_{\mathrm{a},K,i}^{k,n,m}\big)^2$; for $\mathrm{a} = \mathrm{tm}$, the dependence of the estimators on time is left implicit. The global versions, like in (6.7a) but without the initial condition, are

$$\begin{aligned}\eta_{\mathrm{a}}^{k,m} :=& \sqrt{\frac{L_\varphi}{2}}\Bigg(\bigg\{\sum_{n=1}^{N}\Big(\eta_{\mathrm{a}}^{k,n,m}\Big)^2\bigg\}^{\frac12} + \sqrt{2}\bigg\{\sum_{n=1}^{N}\tau^n\sum_{l=1}^{n}\Big(\eta_{\mathrm{a}}^{k,l,m}\Big)^2\bigg\}^{\frac12} \\ &+ \sqrt{2}\bigg\{\sum_{n=1}^{N}\sum_{l=1}^{n}J_{nl}\sum_{q=1}^{l}\Big(\eta_{\mathrm{a}}^{k,q,m}\Big)^2\bigg\}^{\frac12}\Bigg) + \delta_{\mathrm{a}}\|\tilde{u}_{h\tau}^{k,m} - s_{h\tau}^{k,m}\|_\sharp,\end{aligned} \tag{7.4}$$

where $\delta_{\mathrm{a}} = 0$ for $\mathrm{a} = \mathrm{tm}, \mathrm{dd}, \mathrm{lin}$ and δ_{sp} will take the values 0 or 1, depending on the norm in which the error is measured. Then using estimates (6.6) and (6.4) together with the triangle inequality gives:

corollary 7.1 (A posteriori error estimate distinguishing error components)**.** *Let the assumptions of Theorem 6.1 be satisfied. Let the linearized flux $\boldsymbol{\ell}_h^{k,n,m}$ be given by* (7.1) *and the estimators by* (6.7b) *and* (7.2)–(7.4)*. Then, with $\delta_{\mathrm{sp}} = 0$,*

$$\|u - s_{h\tau}^{k,m}\|_\flat \le \sqrt{\frac{L_\varphi}{2}}\sqrt{2e^T-1}\eta_{\mathrm{IC}}^{k,m} + \eta_{\mathrm{sp}}^{k,m} + \eta_{\mathrm{tm}}^{k,m} + \eta_{\mathrm{dd}}^{k,m} + \eta_{\mathrm{lin}}^{k,m},$$

and, under condition (6.5) *and with $\delta_{\mathrm{sp}} = 1$,*

$$\|u - \tilde{u}_{h\tau}^{k,m}\|_\sharp \le \sqrt{\frac{L_\varphi}{2}}\sqrt{2e^T-1}\eta_{\mathrm{IC}}^{k,m} + \eta_{\mathrm{sp}}^{k,m} + \eta_{\mathrm{tm}}^{k,m} + \eta_{\mathrm{dd}}^{k,m} + \eta_{\mathrm{lin}}^{k,m}.$$

8 Stopping criteria and optimal balancing of the different error components

We provide here stopping criteria for the OSWR algorithm and the nonlinear solver for the subdomain problems as in [25, 17, 22, 3] and the references therein.

Let two real parameters δ_{lin} and δ_{dd} be given in $(0,1)$. The stopping criteria for the linearization step (inner loop in m) in each subdomain i, at each time step n, and each OSWR iteration k is chosen as, employing the estimates (7.3)

$$\eta_{\mathrm{lin},i}^{k,n,m} \le \delta_{\mathrm{lin}} \max\Big\{\eta_{\mathrm{sp},i}^{k,n,m}, \eta_{\mathrm{tm},i}^{k,n,m}, \eta_{\mathrm{dd},i}^{k,n,m}\Big\}, \quad i = 1,2. \tag{8.1}$$

Similarly, the stopping criteria for the OSWR algorithm (outer loop in k) is set as, employing the estimates (7.4),

$$\eta_{\mathrm{dd}}^{k,m} \le \delta_{\mathrm{dd}} \max\Big\{\eta_{\mathrm{sp}}^{k,m}, \eta_{\mathrm{tm}}^{k,m}\Big\}. \tag{8.2}$$

The first criterion (8.1) stipulates that there is no need to continue with the linearization iterations if the overall error is dominated by the other components. That of the second criterion (8.2) decides that we stop the OSWR algorithm if the domain decomposition error is dominated by one of the other components. The entire procedure of the approach is then described by the following algorithm:

Data: Enter T, u_0, and Ω_i, π_i, λ_i, and f_i, $i = 1, 2$.
Result: The saturations $u_{h\tau,i}^{k,m}$.
Give the initial Ventcell guess $\Psi_i^{0,1}$, $i = 1, 2$, on Γ;
$k := 0$;
repeat
  $k \longleftarrow k + 1$;
  for *i=1,2* **do**
    $j := (3 - i)$;
    $n := 0$;
    while $t^n \leq T$ **do**
      $n \longleftarrow n + 1$;
      $m := 0$;
      repeat
        $m \longleftarrow m + 1$;
        $u_{h,i}^{k,n,m} := \Upsilon_i(u_{h,i}^{k,n,m-1}, \Psi_j^{k-1,n}, f_i^n, u_{h,i}^{k,n-1})$ by (4.4);
        Compute $\eta_{\mathrm{sp},i}^{k,n,m}$, $\eta_{\mathrm{tm},i}^{k,n,m}$, $\eta_{\mathrm{dd},i}^{k,n,m}$, and $\eta_{\mathrm{lin},i}^{k,n,m}$;
      until $\eta_{\mathrm{lin},i}^{k,n,m} \leq \delta_{\mathrm{lin}} \max\left\{\eta_{\mathrm{sp},i}^{k,n,m}, \eta_{\mathrm{tm},i}^{k,n,m}, \eta_{\mathrm{dd},i}^{k,n,m}\right\}$;
      Set $u_{h,i}^{k,n} := u_{h,i}^{k,n,m}$;
      Set $\Psi_i^{k-1,n} := \{\Psi_{L,\sigma}^{k-1,n}\}_{\sigma=K|L,K\in\mathcal{T}_{h,i},L\in\mathcal{T}_{h,j}}$ with, by (4.3),
      $\Psi_{L,\sigma}^{k-1,n} := F_{L,\sigma}(u_{h,j}^{k-1,n}) + \gamma_{i,j}\dfrac{\Pi_j(u_{L,\sigma}^{k-1,n}) - \Pi_j(u_{L,\sigma}^{k-1,n-1})}{\tau^n}|\sigma| + \left(\Lambda_{L,\Gamma}(u_{h,j}^{k-1,n})\right)_\sigma$;
    end
  end
  Compute $\eta_{\mathrm{sp}}^{k,m}$, $\eta_{\mathrm{tm}}^{k,m}$, $\eta_{\mathrm{dd}}^{k,m}$;
until $\eta_{\mathrm{dd}}^{k,m} \leq \delta_{\mathrm{dd}} \max\left\{\eta_{\mathrm{sp}}^{k,m}, \eta_{\mathrm{tm}}^{k,m}\right\}$;

Algorithm 1: Complete solution algorithm with adaptive stopping criteria

Remark 8.1 (Space and time adaptivity)**.** *The above local-in-time estimators are calculated on each element of the mesh and on each time step, and could also be used as indicators in order to refine adaptively the time steps τ^n and/or the space meshes $\mathcal{T}_{h,i}$, see [22, 17, 49] and the references therein.*

9 Numerical experiments

In this section we illustrate the efficiency of our theoretical results on a numerical experiment with the finite volume OSWR algorithm of Section 4. We take $\Omega = [0, 1]^3$ and $T = 15$. The subdomains are $\Omega_1 = \{0 < x < 1/2\}$ and $\Omega_2 = \{1/2 < x < 1\}$, with $\Gamma = \{x = 1/2\}$. We consider the capillary pressure functions and the global mobilities from [23] given respectively by

$$\pi_1(u) = 5u^2, \qquad \pi_2(u) = 5u^2 + 1, \qquad \lambda_i(u) = u(1 - u),\ i \in \{1, 2\}. \tag{9.1}$$

We impose Dirichlet conditions on two subsets of the boundary $\partial\Omega$. A saturation is set equal to 0.9 on $\Gamma_{\mathrm{D,in}} = \{(x, y, z) \in \partial\Omega \mid x = 0 \text{ and } 0.4 \leq y \leq 0.6\}$. On the outflow boundary $\Gamma_{\mathrm{out}} = \{(x, y, z) \in \partial\Omega \mid x = 1\}$, the saturation at time t^{n+1} is set equal to that inside the closest cell at time t^n (see [1]). We assume homogeneous Neumann boundary conditions on the remaining part of the boundary. The initial condition is taken to be zero everywhere, which fits (2.6a) and consequently (2.10a) at the interface between the rocks. We take $f = 0$ in Ω_1 and Ω_2. The gas is moving through the interface Γ before penetrating the subdomain Ω_2. Note that the gas cannot enter the subdomain Ω_2 if the capillary pressure $\pi_1(u_1)$ is lower than the

entry pressure $\pi_1(u_1^*)$, with $u_1^* = \dfrac{1}{\sqrt{5}}$.

For the spatial discretization, we use uniform meshes in the subdomains consisting of rectangular parallelepipeds matching on the interface Γ. The implementation is based on the Matlab Reservoir Simulation Toolbox [37], and makes use of its automatic differentiation feature to compute the Jacobian matrices for solving the nonlinear subdomain problems by Newton's method. The optimized (Robin or Ventcell) parameters are computed by numerically minimizing the continuous convergence factor corresponding to a linearized version of the problem (see [2] for details).

In the rest of this section, we denote the method defined by using the OSWR method with Robin transmission conditions by Robin-OSWR, while the method using full Ventcell transmission conditions will be denoted by Ventcell-OSWR. When appropriate, we qualify the Robin conditions as one-sided ($\alpha_{12} = \alpha_{21}$) or two-sided in the more general case.

9.1 The performance of the OSWR method with adaptive stopping criteria

We start by analyzing the performance of the OSWR algorithm with adaptive stopping criteria of Section 8. We in particular compare (8.2) with the common approach in which the OSWR algorithm is continued until the residual on the interface becomes smaller than a threshold taken as 10^{-6}, i.e.,

$$\|\Psi_1^k - \Psi_1^{k-1}\|_{\infty,\Gamma} + \|\Psi_2^k - \Psi_2^{k-1}\|_{\infty,\Gamma} \leq 10^{-6}. \tag{9.2}$$

The Newton iterations are stopped when the residuals in both subdomains Ω_i satisfy

$$\|\varphi_i(u_{h,i}^{k,n,m}) - \varphi_i(u_{h,i}^{k,n,m-1})\|_{\infty,\Omega_i} \leq 10^{-8}. \tag{9.3}$$

In this first experiment, we consider the OSWR algorithm with Robin transmission conditions, i.e. $\gamma_{12} = \gamma_{21} = 0$ and $\alpha = \alpha_{1,2} = \alpha_{2,1}$. Four snapshots of the saturation are shown in Fig. 5, together with two snapshots of the capillary pressure in Fig. 6. As expected, the saturation of the gas in Ω_1, as well as the capillary pressure, increase until the capillary pressure reaches the entry pressure. We can see that the capillary pressure field becomes continuous when the entry pressure is reached, then Ω_2 is infiltrated by the gas, but the saturation remains discontinuous across the interface and some quantity of gas remains trapped under the rock discontinuity.

Next we verify the performance of the optimized parameters. Fig. 7 (left) shows the domain decomposition estimator $\eta_{\mathrm{dd}}^{k,m}$ after $k = 25$ OSWR iterations as a function of the Robin parameter α. The estimator behaves very similarly to what is usually observed for the DD error (see e.g. [28]). Moreover, the optimized parameter (marked by a square) is close to the numerically optimal value. This result points the way to the possibility of finding the optimal Robin parameter by minimizing the DD estimator. It also confirms the efficiency of the DD estimator to separate the domain decomposition error from the other components of the global error.

In Fig. 7 (right), we plot the dependence of the different estimators on the OSWR iterations. The adaptive stopping criterion (8.2) needs only 10 iterations, while the classical stopping criterion (9.2) requires 25 iterations.

Fig. 8 depicts the evolution of the estimated error after using the stopping criteria (8.2) with $\delta_{\mathrm{dd}} = 0.1$ and (8.1) with $\delta_{\mathrm{lin}} = 0.1$. We notice that the error distribution follows the saturation front but also that some error near the interface is still detected. In Fig. 9, the domain decomposition error is shown at two different time steps, and clearly one can remark that the DD error is not affecting the global error, in agreement with (8.2). The results, from a practical viewpoint, coincide with the results obtained using classical stopping criteria (9.3) and (9.2).

Fig. 10 plots the different estimators in each subdomain, as a function of the Newton iteration at the final iteration of OSWR algorithm. Only three iterations are required to reach (8.1) for the subdomain solvers, where 13 iterations for the solves in Ω_1 and 7 iterations for the solves in Ω_2 are needed to reach the classical criteria (9.3).

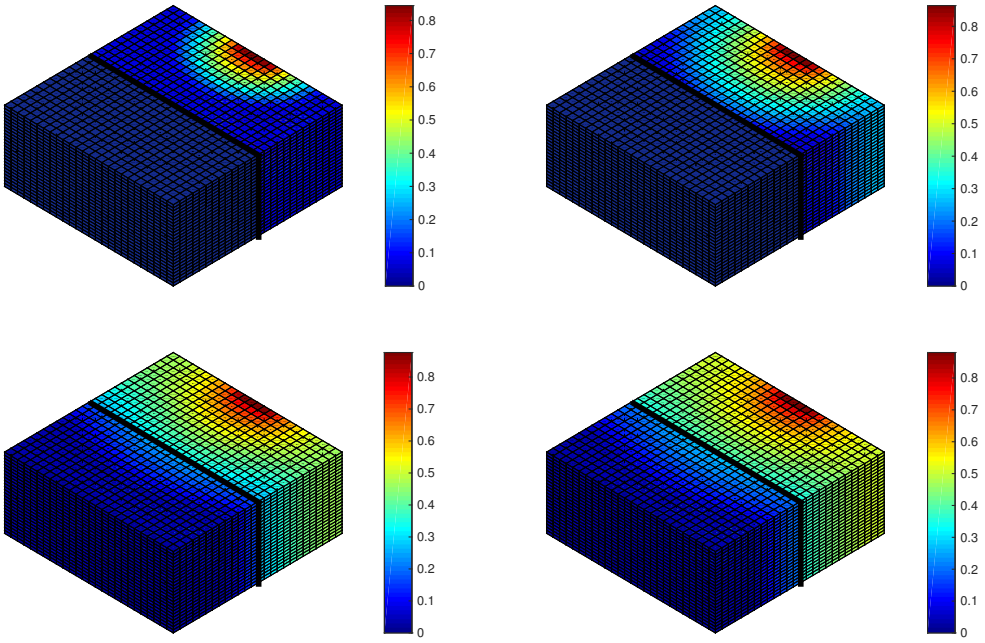

Figure 5: Robin interface conditions: saturation $u(t)$ for $t = 2.9$, $t = 6.6$, $t = 13$, and $t = 15$

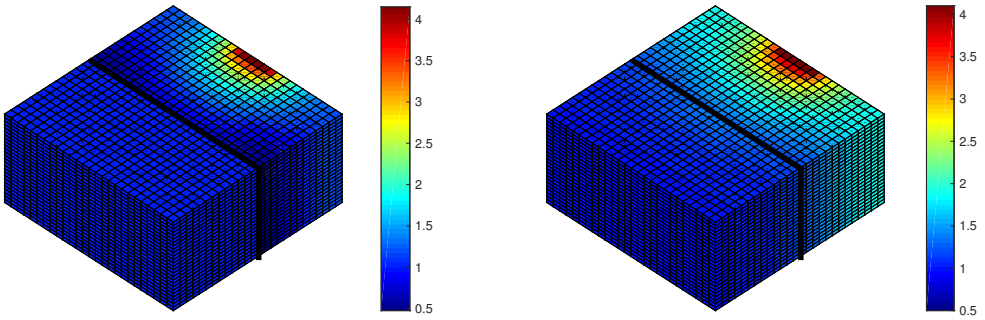

Figure 6: Robin interface conditions: capillary pressure field $\pi(u(t), \cdot)$ for $t = 6.6$ and $t = 15$

9.2 Comparison of Robin- and Ventcell-OSWR algorithm with adaptive stopping criteria

We now consider the OSWR algorithm with two-sided Robin transmission conditions (i.e. $\gamma_{12} = \gamma_{21} = 0$ and $\alpha_{12} \neq \alpha_{21}$) on the one hand, and Ventcell transmission conditions (i.e. $\gamma = \gamma_{12} = \gamma_{21}$ and $\alpha = \alpha_2 = \alpha_{21}$) on the other hand. Fig. 11 shows, for each method, the dependence of the different estimators on the number of DD iterations. We observe that the estimated space and time errors coincide for the two methods and that they are also very close to those obtained with the one-sided Robin-OSWR algorithm (see Fig. 7), as expected. For the DD error, both methods are faster than the one-sided Robin-OSWR method. The usual stopping criteria are reached after 14 and 9 iterations respectively, whereas only 4 iterations are needed with the adaptive stopping criteria 8.2. Fig. 12 shows contour lines of the DD estimator $\eta_{\mathrm{dd}}^{k,m}$ as a function of the parameters, at the final OSWR iteration. The square marks the parameters obtained via the optimization procedure described previously. It is worth noting that this optimized parameter is close to the parameter that numerically minimizes the error estimate $\eta_{\mathrm{dd}}^{k,m}$.

We have also checked the efficiency of the adaptive linearization stopping criterion (8.1) for both methods.

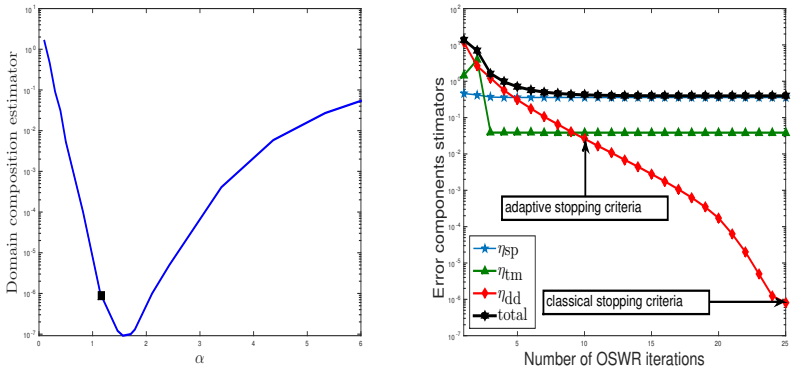

Figure 7: Domain decomposition error estimator $\eta_{\mathrm{dd}}^{k,m}$ after $k = 25$ Robin-OSWR iterations as a function of the parameter α (left) and evolution of the spatial, temporal, and domain decomposition error estimators as a function of the number of Robin-OSWR iterations (right)

The results (not shown here) are similar to the Robin-OSWR case, which allows to stop the Newton algorithm after 4 iterations for most of the solves, instead of 8 and 15 for the classical criterion.

The results confirm that the domain decomposition estimator is a practical tool to estimate the domain decomposition error component and that combining optimized parameters and adaptive stopping criteria results in efficient OSWR algorithms.

Acknowledgments

This work is the result of a collaboration that took place during the CEMRACS summer school & projects 2016. We warmly thank the organizers as well as the CIRM for its welcome.

References

[1] E. Ahmed, J. Jaffré, and J. E. Roberts, *A reduced fracture model for two-phase flow with different rock types*, Math. Comput. Simulation, 137 (2017), pp. 49–70, https://doi.org/10.1016/j.matcom.2016.10.005, http://dx.doi.org/10.1016/j.matcom.2016.10.005.

[2] E. Ahmed, C. Japhet, and M. Kern, *A finite volume Schwarz algorithm for two-phase immiscible flow with different rock types*. In preparation.

[3] S. Ali Hassan, *A posteriori error estimates and stopping criteria for solvers using domain decomposition method and with local time stepping*. Submitted Ph.D. thesis, University Paris 6, 2017.

[4] S. Ali Hassan, C. Japhet, M. Kern, and M. Vohralík, *A posteriori stopping criteria for optimized Schwarz domain decomposition algorithms in mixed formulations*. HAL Preprint 01529532, submitted for publication, 2017, https://hal.inria.fr/hal-01529532.

[5] B. Andreianov, K. Brenner, and C. Cancès, *Approximating the vanishing capillarity limit of two-phase flow in multi-dimensional heterogeneous porous medium*, ZAMM Z. Angew. Math. Mech., 94 (2014), pp. 655–667, https://doi.org/10.1002/zamm.201200218, http://dx.doi.org/10.1002/zamm.201200218.

[6] M. Arioli, D. Loghin, and A. J. Wathen, *Stopping criteria for iterations in finite element methods*, Numer. Math., 99 (2005), pp. 381–410, https://doi.org/10.1007/s00211-004-0568-z, http://dx.doi.org/10.1007/s00211-004-0568-z.

[7] K. Aziz and A. Settari, *Petroleum Reservoir Simulation*, Applied Science Publishers, 1979, http://amazon.com/o/ASIN/B0083K23YA.

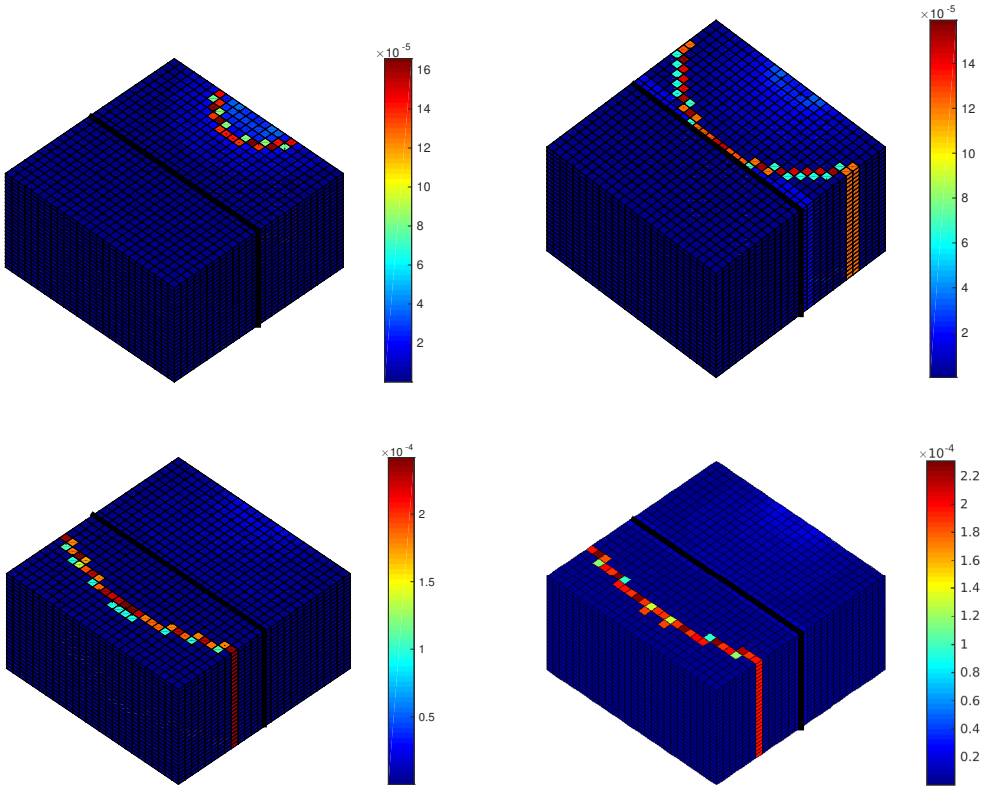

Figure 8: Robin interface conditions: estimated error for $t = 2.9$, $t = 6.6$, $t = 13$, and $t = 15$

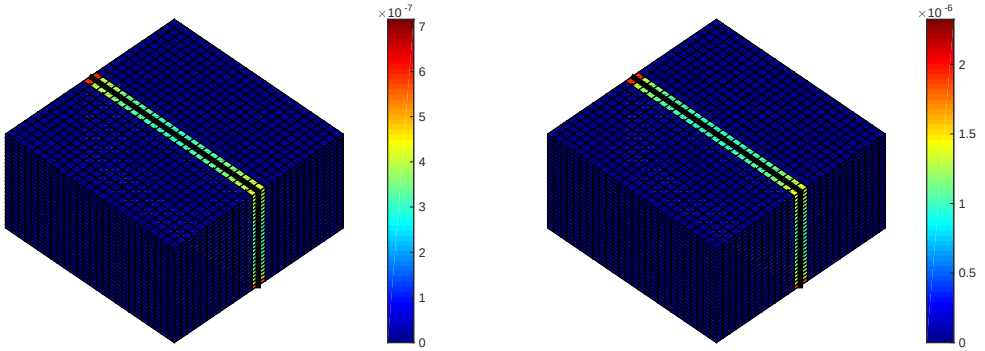

Figure 9: Robin interface conditions: estimated DD error for $t = 6.6$ and $t = 15$

[8] R. Becker, C. Johnson, and R. Rannacher, *Adaptive error control for multigrid finite element methods*, Computing, 55 (1995), pp. 271–288, https://doi.org/10.1007/BF02238483, http://dx.doi.org/10.1007/BF02238483.

[9] D. Bennequin, M. J. Gander, and L. Halpern, *A homographic best approximation problem with application to optimized Schwarz waveform relaxation*, Math. Comp., 78 (2009), pp. 185–223, https://doi.org/10.1090/S0025-5718-08-02145-5.

[10] H. Berninger, S. Loisel, and O. Sander, *The 2-Lagrange multiplier method applied to nonlinear transmission problems for the Richards equation in heterogeneous soil with cross points*, SIAM J. Sci.

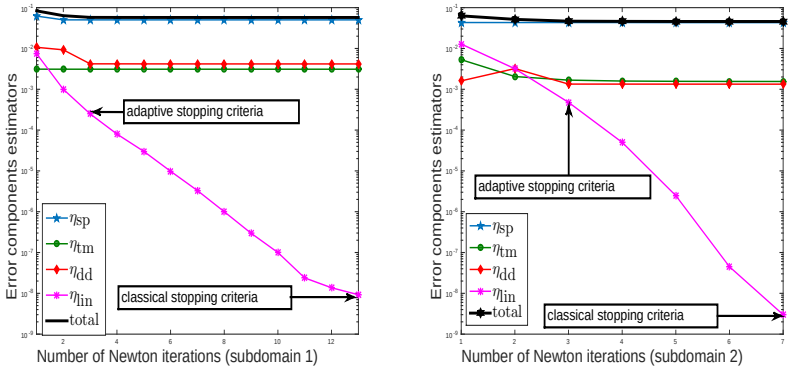

Figure 10: Robin interface conditions: evolution of the spatial, temporal, domain decomposition, and linearization error estimators as a function of Newton iterations for the final iteration of OSWR algorithm for $t = 6.6$; subdomain 1 (left) and subdomain 2 (right)

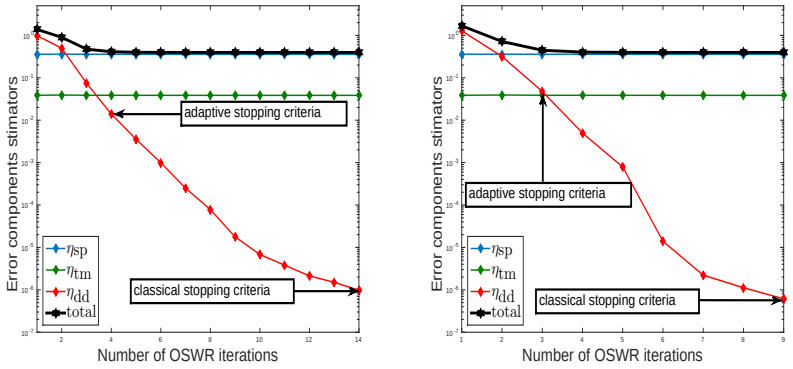

Figure 11: Spatial, temporal, and domain decomposition error estimators as a function of OSWR iterations for the two-sided Robin-OSWR method (left) and the Ventcell-OSWR method (right)

Comput., 36 (2014), pp. A2166–A2198, https://doi.org/10.1137/120901064, http://dx.doi.org/10.1137/120901064.

[11] H. Berninger and O. Sander, *Substructuring of a Signorini-type problem and Robin's method for the Richards equation in heterogeneous soil*, Comput. Vis. Sci., 13 (2010), pp. 187–205, https://doi.org/10.1007/s00791-010-0141-5, http://dx.doi.org/10.1007/s00791-010-0141-5.

[12] K. Brenner, C. Cancès, and D. Hilhorst, *Finite volume approximation for an immiscible two-phase flow in porous media with discontinuous capillary pressure*, Comput. Geosci., 17 (2013), pp. 573–597, https://doi.org/10.1007/s10596-013-9345-3, http://dx.doi.org/10.1007/s10596-013-9345-3.

[13] F. Caetano, M. J. Gander, L. Halpern, and J. Szeftel, *Schwarz waveform relaxation algorithms for semilinear reaction-diffusion equations*, Netw. Heterog. Media, 5 (2010), pp. 487–505, https://doi.org/10.3934/nhm.2010.5.487, http://dx.doi.org/10.3934/nhm.2010.5.487.

[14] C. Cancès, *Nonlinear parabolic equations with spatial discontinuities*, NoDEA Nonlinear Differential Equations Appl., 15 (2008), pp. 427–456, https://doi.org/10.1007/s00030-008-6030-7, http://dx.doi.org/10.1007/s00030-008-6030-7.

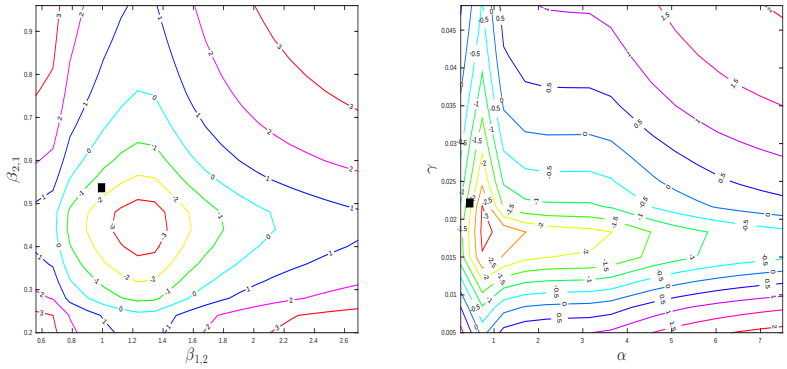

Figure 12: Domain decomposition error estimator $\eta_{\mathrm{dd}}^{k,m}$ as a function of the free parameters after 4 iterations of the OSWR of the two-sided Robin-OSWR method (left) and 3 iterations of the optimized Ventcell-OSWR method (right)

[15] C. Cancès, *Finite volume scheme for two-phase flows in heterogeneous porous media involving capillary pressure discontinuities*, M2AN Math. Model. Numer. Anal., 43 (2009), pp. 973–1001, https://doi.org/10.1051/m2an, http://dx.doi.org/10.1051/m2an/2009032.

[16] C. Cancès, T. Gallouët, and A. Porretta, *Two-phase flows involving capillary barriers in heterogeneous porous media*, Interfaces Free Bound., 11 (2009), pp. 239–258, https://doi.org/10.4171/IFB, http://dx.doi.org/10.4171/IFB/210.

[17] C. Cancès, I. S. Pop, and M. Vohralík, *An a posteriori error estimate for vertex-centered finite volume discretizations of immiscible incompressible two-phase flow*, Math. Comp., 83 (2014), pp. 153–188, https://doi.org/10.1090/S0025-5718-2013-02723-8, http://dx.doi.org/10.1090/S0025-5718-2013-02723-8.

[18] G. Chavent and J. Jaffré, *Mathematical models and finite elements for reservoir simulation*, North-Holland, Amsterdam, 1986. Studies in Mathematics and Its Applications, Vol. 17.

[19] Y. Chen and W. Liu, *A posteriori error estimates of mixed methods for miscible displacement problems*, Internat. J. Numer. Methods Engrg., 73 (2008), pp. 331–343, https://doi.org/10.1002/nme.2075, http://dx.doi.org/10.1002/nme.2075.

[20] L. C. Cowsar, J. Mandel, and M. F. Wheeler, *Balancing domain decomposition for mixed finite elements*, Math. Comp., 64 (1995), pp. 989–1015, https://doi.org/10.2307/2153480, http://dx.doi.org/10.2307/2153480.

[21] D. A. Di Pietro, E. Flauraud, M. Vohralík, and S. Yousef, *A posteriori error estimates, stopping criteria, and adaptivity for multiphase compositional Darcy flows in porous media*, J. Comput. Phys., 276 (2014), pp. 163–187, https://doi.org/10.1016/j.jcp.2014.06.061, http://dx.doi.org/10.1016/j.jcp.2014.06.061.

[22] D. A. Di Pietro, M. Vohralík, and S. Yousef, *Adaptive regularization, linearization, and discretization and a posteriori error control for the two-phase Stefan problem*, Math. Comp., 84 (2015), pp. 153–186, https://doi.org/10.1090/S0025-5718-2014-02854-8, http://dx.doi.org/10.1090/S0025-5718-2014-02854-8.

[23] G. Enchéry, R. Eymard, and A. Michel, *Numerical approximation of a two-phase flow problem in a porous medium with discontinuous capillary forces*, SIAM J. Numer. Anal., 43 (2006), pp. 2402–2422, https://doi.org/10.1137/040602936, http://dx.doi.org/10.1137/040602936.

[24] A. Ern and M. Vohralík, *A posteriori error estimation based on potential and flux reconstruction for the heat equation*, SIAM J. Numer. Anal., 48 (2010), pp. 198–223, https://doi.org/10.1137/090759008, http://dx.doi.org/10.1137/090759008.

[25] A. Ern and M. Vohralík, *Adaptive inexact Newton methods with a posteriori stopping criteria for nonlinear diffusion PDEs*, SIAM J. Sci. Comput., 35 (2013), pp. A1761–A1791, https://doi.org/10.1137/120896918, http://dx.doi.org/10.1137/120896918.

[26] R. Eymard, T. Gallouët, and R. Herbin, *Finite volume methods*, in Handbook of Numerical Analysis, Vol. VII, , North-Holland, Amsterdam, 2000, pp. 713–1020.

[27] R. Eymard, T. Gallouët, and R. Herbin, *Finite volume approximation of elliptic problems and convergence of an approximate gradient*, Appl. Numer. Math., 37 (2001), pp. 31–53, https://doi.org/10.1016/S0168-9274(00)00024-6, http://dx.doi.org/10.1016/S0168-9274(00)00024-6.

[28] M. J. Gander, *Optimized Schwarz methods*, SIAM J. Numer. Anal., 44 (2006), pp. 699–731.

[29] B. Ganis, K. Kumar, G. Pencheva, M. F. Wheeler, and I. Yotov, *A global Jacobian method for mortar discretizations of a fully implicit two-phase flow model*, Multiscale Model. Simul., 12 (2014), pp. 1401–1423, https://doi.org/10.1137/140952922, http://dx.doi.org/10.1137/140952922.

[30] F. Haeberlein, L. Halpern, and A. Michel, *Newton-Schwarz optimised waveform relaxation Krylov accelerators for nonlinear reactive transport*, in Domain decomposition methods in science and engineering XX, vol. 91 of Lect. Notes Comput. Sci. Eng., Springer, Heidelberg, 2013, pp. 387–394, https://doi.org/10.1007/978-3-642-35275-1_45, http://dx.doi.org/10.1007/978-3-642-35275-1_45.

[31] L. Halpern and F. Hubert, *A finite volume Ventcell-Schwarz algorithm for advection-diffusion equations*, SIAM J. Numer. Anal., 52 (2014), pp. 1269–1291, https://doi.org/10.1137/130919799, http://dx.doi.org/10.1137/130919799.

[32] T.-T.-P. Hoang, J. Jaffré, C. Japhet, M. Kern, and J. E. Roberts, *Space-time domain decomposition methods for diffusion problems in mixed formulations*, SIAM J. Numer. Anal., 51 (2013), pp. 3532–3559, https://doi.org/10.1137/130914401, http://dx.doi.org/10.1137/130914401.

[33] T. T. P. Hoang, C. Japhet, M. Kern, and J. E. Roberts, *Ventcell conditions with mixed formulations for flow in porous media*, in Decomposition Methods in Science and Engineering XXII, T. Dickopf, M. Gander, L. Halpern, R. Krause, and L. F. Pavarino, eds., vol. 104 of Lecture Notes in Computational Science and Engineering, Springer, 2016, pp. 531–540.

[34] C. Japhet and F. Nataf, *The best interface conditions for domain decomposition methods: absorbing boundary conditions*, in Absorbing Boundaries and Layers, Domain Decomposition Methods, Nova Sci. Publ., Huntington, NY, 2001, pp. 348–373.

[35] P. Jiránek, Z. Strakoš, and M. Vohralík, *A posteriori error estimates including algebraic error and stopping criteria for iterative solvers*, SIAM J. Sci. Comput., 32 (2010), pp. 1567–1590, https://doi.org/10.1137/08073706X, http://dx.doi.org/10.1137/08073706X.

[36] K. Y. Kim, *A posteriori error estimators for locally conservative methods of nonlinear elliptic problems*, Appl. Numer. Math., 57 (2007), pp. 1065–1080, https://doi.org/10.1016/j.apnum.2006.09.010, http://dx.doi.org/10.1016/j.apnum.2006.09.010.

[37] K.-A. Lie, S. Krogstad, I. S. Ligaarden, J. R. Natvig, H. M. Nilsen, and B. Skaflestad, *Open source matlab implementation of consistent discretisations on complex grids*, Comput. Geosci., 16 (2012), pp. 297–322, https://doi.org/10.1007/s10596-011-9244-4.

[38] V. Martin, *An optimized Schwarz waveform relaxation method for the unsteady convection diffusion equation in two dimensions*, Appl. Numer. Math., 52 (2005), pp. 401–428, https://doi.org/10.1016/j.apnum.2004.08.022, http://dx.doi.org/10.1016/j.apnum.2004.08.022.

[39] R. H. Nochetto, A. Schmidt, and C. Verdi, *A posteriori error estimation and adaptivity for degenerate parabolic problems*, Math. Comp., 69 (2000), pp. 1–24.

[40] G. V. Pencheva, M. Vohralík, M. F. Wheeler, and T. Wildey, *Robust a posteriori error control and adaptivity for multiscale, multinumerics, and mortar coupling*, SIAM J. Numer. Anal., 51 (2013), pp. 526–554, https://doi.org/10.1137/110839047.

[41] I. S. Pop, J. Bogers, and K. Kumar, *Analysis and upscaling of a reactive transport model in fractured porous media with nonlinear transmission condition*, Vietnam J. Math., 45 (2017), pp. 77–102, https://doi.org/10.1007/s10013-016-0198-7, http://dx.doi.org/10.1007/s10013-016-0198-7.

[42] V. Rey, P. Gosselet, and C. Rey, *Strict lower bounds with separation of sources of error in non-overlapping domain decomposition methods*, Internat. J. Numer. Methods Engrg., 108 (2016), pp. 1007–1029, https://doi.org/10.1002/nme.5244, http://dx.doi.org/10.1002/nme.5244.

[43] V. Rey, C. Rey, and P. Gosselet, *A strict error bound with separated contributions of the discretization and of the iterative solver in non-overlapping domain decomposition methods*, Comput. Methods Appl. Mech. Engrg., 270 (2014), pp. 293–303, https://doi.org/10.1016/j.cma.2013.12.001, http://dx.doi.org/10.1016/j.cma.2013.12.001.

[44] J. O. Skogestad, E. Keilegavlen, and J. M. Nordbotten, *Domain decomposition strategies for nonlinear flow problems in porous media*, J. Comput. Phys., 234 (2013), pp. 439–451, https://doi.org/10.1016/j.jcp.2012.10.001, http://dx.doi.org/10.1016/j.jcp.2012.10.001.

[45] J. O. Skogestad, E. Keilegavlen, and J. M. Nordbotten, *Two-scale preconditioning for two-phase nonlinear flows in porous media*, Transp. Porous Media, 114 (2016), pp. 485–503, https://doi.org/10.1007/s11242-015-0587-5, http://dx.doi.org/10.1007/s11242-015-0587-5.

[46] C. J. Van Duijn, J. Molenaar, and M. J. De Neef, *The effect of capillary forces on immiscible two-phase flow in heterogeneous porous media*, Transport in Porous Media, 21 (1995), pp. 71–93, https://doi.org/10.1007/BF00615335, http://dx.doi.org/10.1007/BF00615335.

[47] R. Verfürth, *A posteriori error estimates for finite element discretizations of the heat equation*, Calcolo, 40 (2003), pp. 195–212, https://doi.org/10.1007/s10092-003-0073-2, http://dx.doi.org/10.1007/s10092-003-0073-2.

[48] M. Vohralík, *Unified primal formulation-based a priori and a posteriori error analysis of mixed finite element methods*, Math. Comp., 79 (2010), pp. 2001–2032, https://doi.org/10.1090/S0025-5718-2010-02375-0, http://dx.doi.org/10.1090/S0025-5718-2010-02375-0.

[49] M. Vohralík and M. F. Wheeler, *A posteriori error estimates, stopping criteria, and adaptivity for two-phase flows*, Comput. Geosci., 17 (2013), pp. 789–812, https://doi.org/10.1007/s10596-013-9356-0, http://www.springerlink.com/openurl.asp?genre=article&id=doi:10.1007/s10596-013-9356-0.

[50] I. Yotov, *A mixed finite element discretization on non-matching multiblock grids for a degenerate parabolic equation arising in porous media flow*, East-West J. Numer. Math., 5 (1997), pp. 211–230.

[51] I. Yotov, *Interface solvers and preconditioners of domain decomposition type for multiphase flow in multiblock porous media*, in Scientific computing and applications, vol. 7 of Adv. Comput. Theory Pract., Nova Sci. Publ., Huntington, NY, 2001, pp. 157–167.